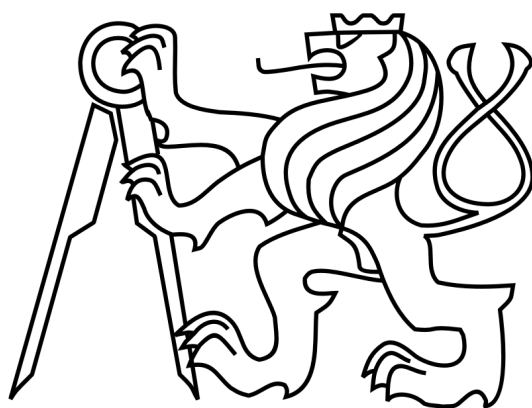


CZECH TECHNICAL UNIVERSITY IN PRAGUE
Faculty of Nuclear Sciences and Physical Engineering
Department of Physics



Bachelor thesis

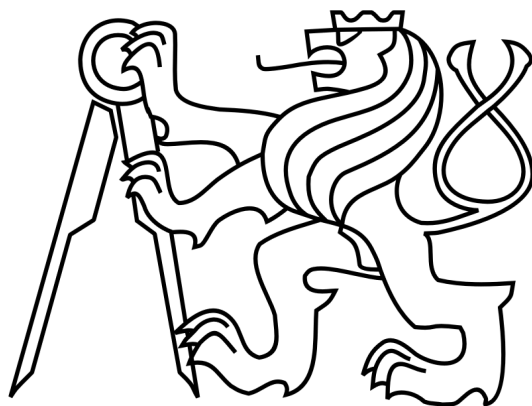
Polarization of quarkonia

Alena Harlenderová

Supervisor: Dr. Barbara Antonina Trzeciak

Prague, 2015

ČESKÁ TECHNICKÁ UNIVERZITA V PRAZE
Fakulta jaderná a fyzikálně inženýrská
Katedra fyziky



Bakalářská práce

Polarizace kvarkonií

Alena Harlenderová

Supervisor: Dr. Barbara Antonina Trzeciak

Praha, 2015

Prohlášení

Prohlašuji, že jsem svou bakalářskou práci vypracovala samostatně a použila jsem pouze podklady (literaturu, software, atd.) uveřejněné v přiloženém seznamu.

Nemám závažný důvod proti užití tohoto školního díla ve smyslu Zákona .121/2000 Sb., o právu autorském, o právech souvisejících s právem autorským a o změně některých zákonů (autorský zákon).

V Praze dne 7.7.2015

Title: **Polarization of quarkonia**

Specialization: Experimental nuclear and particle physics

Sort of project: Bachelor thesis

Supervisor: Dr. Barbara Trzeciak

Abstract: Heavy quarks can form so called quarkonium, the bound state of a heavy quark and its antiquark. Although, the first quarkonium was discovered in 1974, the exact mechanism of quarkonium production is not fully understood. There are many theoretical approaches to describe the production mechanism of quarkonia. They imply different predictions of some physical quantities that can be measured, such as a cross section or a polarization of quarkonia. These quantities play the key role in distinguishing between theoretical models. Basic approaches to quarkonium production mechanism and to quarkonium polarization measurements will be described in the bachelor thesis. Afterwards, performed measurements of quarkonium polarization in pp and $p\bar{p}$ collisions will be discussed.

Key words: quarkonium, quarkonium polarization, production mechanism, pp collisions

Název práce: **Polarizace kvarkonií**

Autor: Alena Harlenderová

Abstrakt: Těžké kvarky mohou tvořit tzv. kvarkonium, vázaný stav těžkého kvarku a jeho antikvarku. Ačkoliv bylo první kvarkonium objeveno v roce 1974, stále není znám přesný mechanismus jejich produkce. Existuje mnoho teoretických přístupů, které se snaží popsat mechanismus produkce a předpovídají hodnoty pozorovatelných veličin jako je účinný průřez nebo polarizace kvarkonií. Ty pak hrají klíčovou roli v rozhodování mezi modely. V této bakalářské práci budou popsány některé modely produkce kvarkonií a základy měření polarizace kvarkonií. Následně budou představena měření polarizace kvarkonií v pp a $p\bar{p}$ srážkách.

Klíčová slova: kvarkonium, polarizace kvarkonií, mechanismus produkce, pp srážky

Acknowledgement

I would like to express my honest gratitude to my supervisor Dr. Barbara Trzeciak for her willingness, professional feedback, sometimes very colourful corrections, patience, patience, patience and for her goodwill to wait for me while I am catching scooter thieves in the middle of a consultation. My big thanks also belong to my family, boyfriend and friends, because they were here when I needed them.

Contents

Introduction	11
1 Short Introduction to Particle Physics	12
1.1 Leptons	14
1.2 Quarks	14
1.3 Higgs Boson	15
1.4 Gravitational Interaction	15
1.5 Electromagnetic Interaction	15
1.6 Weak Interaction	15
1.7 Strong Interaction	16
1.8 Quark-Gluon Plasma	16
2 Quarkonia	19
2.1 Discovery of J/ψ	20
2.2 Discovery of Υ	22
2.3 Quarkonia as the probes of a hot and dense medium in heavy-ion collisions	23
2.4 Other effects altering quarkonia yields	25
3 Quarkonium production mechanism	28
3.1 The colour-evaporation model (CEM)	28
3.2 The colour-singlet model (CSM)	29
3.3 The non-relativistic quantum chromodynamics (NRQCD) approach	29
4 The Polarization of Quarkonia	32
4.1 Reference Frames	33
4.2 Dilepton Decay Angular Distribution	34
4.2.1 The Frame-Invariant Approach	36
5 Measurements of quarkonium polarization in proton-proton and proton-antiproton collisions	41
5.1 J/ψ polarization measurements in pp collisions at $\sqrt{s} = 200$ GeV by the STAR and PHENIX experiments	41

5.2	J/ψ and $\psi(2S)$ polarization measurements in $p\bar{p}$ collisions at $\sqrt{s} = 1.96$ TeV by the CDF experiments	45
5.3	J/ψ polarization measurements in pp collisions at $\sqrt{s} = 7$ TeV by the ALICE experiment	46
5.4	J/ψ polarization measurements in pp collisions at $\sqrt{s} = 7$ TeV by the LHCb experiment	47
5.5	J/ψ and $\psi(2S)$ polarization measurements in pp collisions at $\sqrt{s} = 7$ TeV by the CMS experiment	48
5.6	$\Upsilon(1S)$, $\Upsilon(2S)$ and $\Upsilon(3S)$ polarization measurements in pp collisions at $\sqrt{s} = 7$ TeV by the CMS experiment	50
Conclusion		55

Introduction

Heavy quarks form quarkonia, bound states of heavy quark and its antiquark. Quarkonia are important for studying QCD mechanisms. They are also abundantly used for analyses of collisions. Although, the first quarkonium was discovered in 1974, the exact mechanism of quarkonium production is not fully understood. There are many theoretical models for quarkonium production mechanism. Various theoretical approaches imply different predictions of some physical quantities that can be measured, such as cross section or polarization of quarkonia.

Quarkonia are produced in a superposition different of mechanisms. The production processes may define a subset of possible eigenstates of the angular momentum component J_z . We call this phenomenon the quarkonium polarization [31]. This quantity may play the key role in distinguishing between theoretical models.

Quarkonia are vector mesons, thus they decay to dilepton pair. The total angular distribution of the positive lepton momentum reflects quarkonium quantum numbers. Thus, we can study the quarkonium polarization through the dilepton decay distribution. Basic approaches to quarkonium production mechanism and to quarkonium polarization measurements will be described in the bachelor thesis. Performed measurements of quarkonium polarization in pp and $p\bar{p}$ collisions will be discussed.

The first chapter will be dedicated to short introduction to particle physics. After that, features of quarkonia, discovery of J/ψ and Υ and common use of quarkonia in particle physics will be described. Some models of quarkonium production will be presented in the Chapter 3. The basic theory connected to polarization of quarkonia and its measurement are going to be discussed in fourth chapter. Measurements of quarkonium polarization in pp and $p\bar{p}$ by various experimental facilities are in the fifth chapter.

Chapter 1

Short Introduction to Particle Physics

People think about principles of our world for thousands of years. Some interesting and pioneering theories were pronounced and discussed even in the antiquity. We can mention for example atomism, the theory including idea of no more divisible parts of matter.

Although, some of relevant ideas such as indivisibility of small parts of matter were mentioned still long time ago, people were not able to verify their correctness for long time. However, technological development in last hundred years enabled scientists from many fields to gain great amount of new experimental information and develop further theories. Especially, our acquaintance with the composition of matter was considerably improved.

At the beginning of last century Rutherford led the series of experiments where metal foils were shot by alpha particles. Observed scattering of alpha particles did not correspond to Thompson model, thus Rutherford designed the pioneering theory about positively charged nucleus and electron cloud surrounding it. Particle physics passed long way since this time. Further scientists improved Rutherfords idea, "looked" inside the nucleus and observed even further structure of matter. The great amount of experimental data have been produced by particle colliders such as the Large Hadron Collider or the Relativistic Heavy Ion Collider. Theories are compared to experimental results of many affiliated collaborations. It all have led to development of modern theories such as the Standard Model of particle physics.

The Standard Model attempts to clarify phenomena of the particle physics on the base of properties of small number of elementary particles and interactions between them [54] (page 2). This theory includes three interactions, weak, strong and electromagnetic. The elementary particles, building blocks of matter, are divided into groups according to their properties. The situation is illustrated in the Figure 1.1. Each particle has its antiparticle in the Standard Model. The particle can be its own antiparticle as the case of the photon.

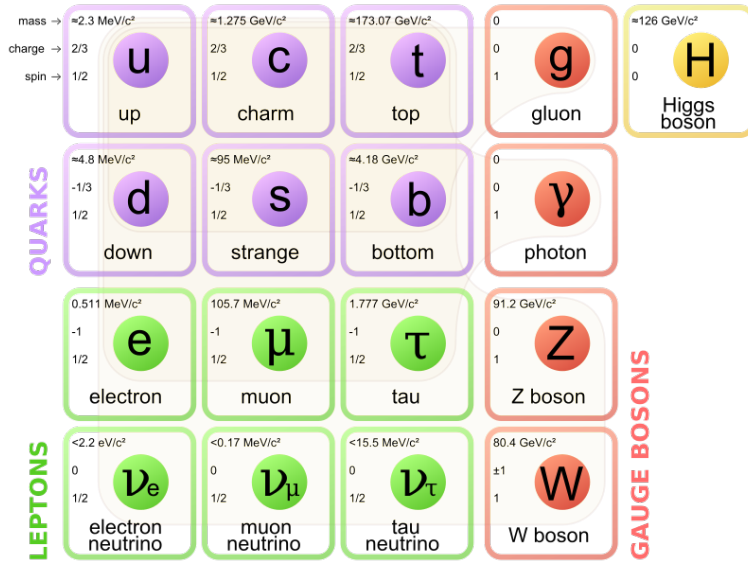


Figure 1.1: Particles of the Standard Model with their masses, charges, spins and flavours. Individual colours differentiate types of particles. Quarks are purple coloured, leptons green coloured, gauge bosons red coloured and the Higgs boson is yellow coloured. Picture is taken from [55].

The particles can be classified according to their spin. Particles with a half-integer spin are called the fermions and their behaviour follows the Fermi-Dirac statistic and the Pauli exclusion principle. An integer spin is attributed to bosons. The bosons obey the Bose-Einstein statistics and do not conform to the Pauli principle.

There are two basic types of elementary fermions in the Standard Model, quarks and leptons. Leptons interact by the weak interaction, whereas quarks also interact strongly. Gauge bosons with spin equal to 1 intermediate the interactions. Z_0 , W^+ and W^- bosons are responsible for the mediation of the weak interaction, photons for the electromagnetic interaction, while gluons for the strong interaction. The Higgs boson is characterized by the spin equal to 0 and does not carry charge [49]. The important property of the Higgs boson is its invariant mass $125.7 \pm 0.4 \text{ GeV}c^{-2}$ [49], which pertains to the highest masses of elementary particles.

Short overview of elementary particles and forces affecting them is going to be described in this chapter. We will focus especially on properties of the strong interaction.

1.1 Leptons

Leptons are group of weakly interacting elementary particles from the Standard Model. They do not interact strongly, since they do not carry any colour.

Three generations of leptons can be observed. First generation comprises of electron e and electron neutrino ν_e , second of muon μ and muon neutrino ν_μ , third of tauon τ and tauon neutrino ν_τ .

Thompson discovered the first lepton, electron, in 1897 [52] (page 45). Electron is characterized by the biggest radiative losses between charged leptons caused by its smallest invariant mass. The probability of emission of photon by muon is approximately 40000 times smaller than the same for electron [28] (page 152). Thus, muons are more penetrating and may fly through Earth's atmosphere. They were firstly observed in cosmic rays.

Charged leptons interact electromagnetically, whereas neutrinos without electric charge interact only weakly. Thus, they are able to penetrate matter easily than other leptons. Electron neutrino was predicted by Pauli in 1930 on the base of properties of electrons from β decay [52] (page 45). Initially, it was assumed that neutrinos are massless. Nevertheless, neutrinos may have invariant mass not equal to zero. It may imply interesting phenomenon, mixing of neutrino flavours [54] (page 39).

1.2 Quarks

Quarks are elementary particles that interact both strongly and weakly. Quarks are divided into three generations similarly as leptons. There are two quarks in each generation, one with charge $\frac{2}{3}$, second with $-\frac{1}{3}$. Each quark carries one colour, quantum number connected to the strong interaction. There are three colours, red (r), green (g) and blue (b), and corresponding anticolours ($\bar{r}, \bar{g}, \bar{b}$) according to the convention.

The first generation comprises of up and down quarks, second of charm and strange quarks, third of top and bottom quarks. Invariant mass of quarks rises with increasing number of a generation. Up and down quark occur commonly in nature. They are bounded for example in protons and neutrons.

Many attempts to observe individual quarks were performed. None of them succeeded, but convincing arguments for their existence were presented. Leptons were scattered from nucleons. High-energy scattering of leptons on protons and neutrons suggested that there exist inner particles [46]. Jet production is also the probe of the existence of quarks [52] (page 121).

Quarks constitute composite particles, hadrons. There are two groups of hadrons, baryons and mesons. Baryons consist either of three quarks or antiquarks. Mesons are bound state of a quark and an antiquark. A quark and an antiquark in a meson can have same flavour. Mesons that consist of heavy quark and its antiquark are called quarkonia.

1.3 Higgs Boson

A scalar field that might be responsible for spontaneous symmetry breaking in gauge theories was proposed [24]. This idea was developed later and it led to the suggestion of existence of the Higgs Boson [24]. The particle production compatible with the Higgs boson was indeed observed by the ATLAS and the CMS experiments at CERN as can be seen in papers [24] and [1].

1.4 Gravitational Interaction

The Gravitational interaction affects all particles with mass. It has infinity reach similarly as the electromagnetic force and can only attract particles. It is believed, that the interaction is mediated by massless type of boson called graviton with the spin 2.

The gravitational interaction is the only one from four basic interactions that is not included in the Standard Model. An unification of all four interactions is considered to be extremely difficult, however few theories with this challenging idea occurred. We can mention for example string theory and its models assumptions, one or more dimensional strings and single parameter, string tension [54] (page 318).

Fortunately, the gravitational interaction can be neglected in the terms of interactions between elementary particles at currently accessible energies [54] (page 2). It has far smaller relative strength in the comparison to the strong interactions than the others at these energies, around 10^{-39} [52] (page 17).

1.5 Electromagnetic Interaction

The electromagnetic interaction affects all particles with charge. There are two types of charge, plus and minus, thus interaction can be both, repulsive and attractive. The interaction is mediated by massless gauge bosons called photons. They do not carry charge, thus they do not interact with other photons. The strength of interaction lies in between the strengths of the strong and the weak interactions at accessible energies and short distances [52] (page 17). This interaction has infinite reach and is not negligible at both subatomic and atomic levels.

The electromagnetic interaction is described within the theory named quantum electrodynamics (QED).

1.6 Weak Interaction

Weak interaction is mediated by exchange of the gauge bosons W^- , W^+ and Z^0 . The invariant mass of W bosons is approximately $80.4 \text{ GeV}c^{-2}$, the invariant mass of Z^0 about $91.2 \text{ GeV}c^{-2}$ [49]. The typical range of the interaction is $2 \cdot 10^{-3} \text{ fm}$ [52] (page 92).

The interaction affects both quarks and leptons. It is allowed to change charge lepton to its neutrino for example. The weak interaction can modify flavour of quarks. We should mention the β decay responsible for transition of the neutron to the proton and the proton to the neutron. The β^+ decay converts an up quark into a down quark by the emission of W^+ . Similarly, during the β^- decay a down quark is changed into an up quark by the emission of W^- .

1.7 Strong Interaction

The strong interaction affects quarks and gluons, but not leptons. The interaction is described within the theory called quantum chromodynamics (QCD). As was mentioned, there are three colours and anticolours which play the role of "charges" in QCD similar to + and - charge in the quantum electrodynamics. Each quark has one of three colours and anticolours.

Mediators of the interaction are massless gauge bosons named gluons. The important difference between the QED and the QCD is that photons do not carry any charge whereas gluons carry the colour. Thus, gluons interact with each other.

The potential between a quark and an antiquark can be represented by the Cornell potential [52] (page 120)

$$V(r) = -\frac{4}{3} \frac{\alpha_s}{r} + kr. \quad (1.1)$$

α_s is the running coupling constant of the strong interaction and depends on the square of transferred fourmomentum Q^2 . Experimentally determined value of α_s depending on momentum transfer Q is depicted in the Figure 1.2. k is the string tension potential, r the distance between a quark and an antiquark.

The second term of the Cornell potential is the string potential. The coefficient k manifests itself at long distances. The potential rises with increasing distance of a quark and an antiquark. If the energy of the potential exceeds the invariant mass of two quarks, a new quark-antiquark pair arises. In other words, it is impossible to simply separate one quark from others and observe it alone. This phenomenon is called the colour confinement [52].

However, strong interacting matter behaves differently at short distances. The first term of the potential is dominant in this case. Nevertheless, also this term tends to zero with decreasing r . Q^2 rises with descending r . Subsequently, the whole first term tends to zero. Thus, quarks in dense matter behave almost as free particles. This phenomenon is called asymptotic freedom. The Q^2 rises also with a temperature.

1.8 Quark-Gluon Plasma

The matter can undergo the phase transition from cold nuclear matter to a dense or/and hot deconfined stage of the matter according to theoretical predictions.

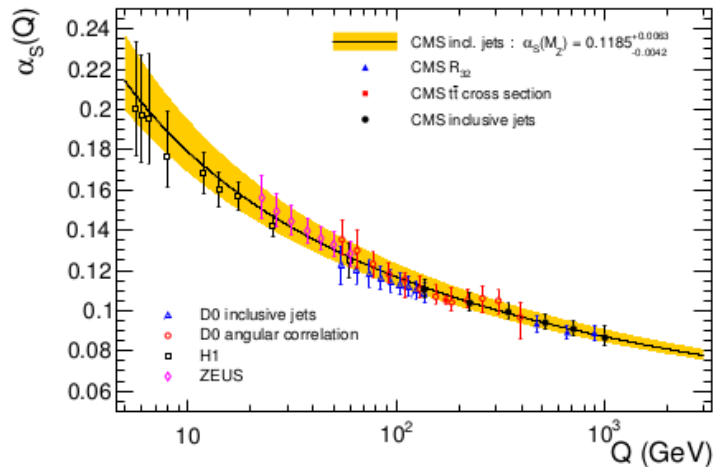


Figure 1.2: The strong coupling constant (band) with total uncertainty (band) depending on the transferred momentum $Q = p_T$. Full marks represent results of the CMS measurements gained by different methods, empty marks outcomes of different experiments at the HERA. The figure is taken from [39].

α_s tends to zero with increasing Q^2 and quarks originally strongly bounded in hadrons commence to be less bounded to each other. At high temperature or/and high net-baryon-density (the density of baryons minus the density of antibaryons), quark and gluon degrees of freedom are liberated [53]. Thus, quarks and gluons behave almost as free particles. This state of matter is called the quark-gluon plasma (QGP). A possible phase diagram with the baryon chemical potential μ_B on the horizontal axis and the temperature T on the vertical axis can be seen in the Figure 1.3. The blue line intersecting the horizontal axis approximately at 1100 MeV depicts the first order-phase transition between the hadron gas and the QGP. The critical temperature increases with the decreasing baryon chemical potential. The lattice QCD predicts existence of the cross-over at a lower baryon chemical potentials and a higher temperatures [53]. The crossover is characterized by smooth phase transition of higher order. The point where the first-order transition changes to the cross-over is named the critical point.

The phase transition is a subject of an extensive experimental research. Nuclear matter is characterized by low temperature and the baryon chemical potential around 900 MeV. These properties are changed for example in heavy ion collisions. It is believed that QGP occurs in high-energy more central heavy ion collisions performed at RHIC and CERN.

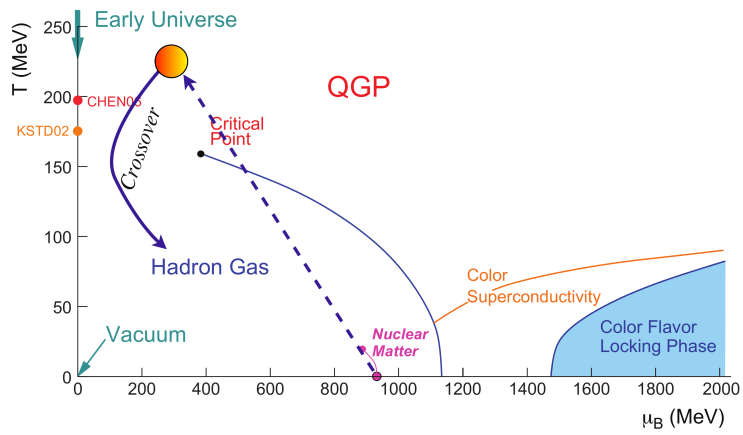


Figure 1.3: The possible phase diagram with the baryon chemical potential μ_B on the horizontal axis and the temperature T on the vertical axis. The Figure is taken from [60].

Chapter 2

Quarkonia

Property of the strong force such as the quark-antiquark potential allows a quark-antiquark pair to create a bound state. Thus, a heavy quark and its antiquark can form so called quarkonium. If the charm quark is bounded with its antiquark, it is called charmonium, in the case of the bottom quark bottomonium. Quarkonia can be observed in many energetical states, which constitute so called "families". The charmonium "family" can be seen in the Figure 2.1. Different states of quarkonia have various quantum numbers such as a parity, an charge conjugation or a total angular momentum.

The most abundantly produced charmonium is J/ψ with the approximate invariant mass of $3.1 \text{ GeV}c^{-2}$ and the same parity (P), charge conjugation (C) and the total angular momentum identical to a photon, $J^{PC} = 1^{--}$ [50] (page 22). J/ψ is a vector meson. Vector mesons may decay to a lepton-antilepton pair.

The discovery of J/ψ was announced by two collaborations the same day. It was the first observed charmed particle. Therefore, we regard the discovery as the discovery of the charm quark. The observation of the heavier state of a vector charmonium $\psi(2S)$ was announced in the same month [6].

A particle with the approximate invariant mass of $9.5 \text{ GeV}c^{-2}$ was observed in the Fermilab [37]. It was the bottomium as was shown later [52]. It was also exposed that the group from the Fermilab observed even three states $\Upsilon(1S)$, $\Upsilon(2S)$ and $\Upsilon(3S)$ with resembling invariant mass during the discovery.

Υ is a vector meson composed of a bottom quark and its antiquark. $\Upsilon(nS)$ refers to a specific energetic state. These states also may decay to a lepton-antilepton pair. Υ is not so abundantly produced as lighter J/ψ because of energetic demands on a creation, thus we usually need considerable number of collisions in comparison to J/ψ for a purpose of an analysis.

A quarkonium production is either prompt or non-prompt. The prompt produced quarkonia originate either from a beginning of a collision or as a result of a decaying of other, higher excited, quarkonium states. For example J/ψ can be produced by decay of heavier charmonium states, as $\psi(2S)$ and χ_c , as is depicted by arrows in the Figure 2.1. Quarkonia from the beginning of the col-

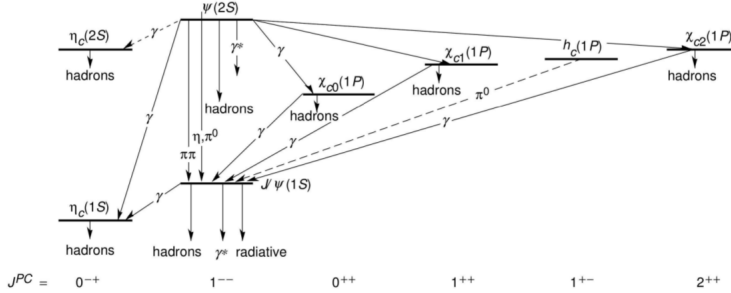


Figure 2.1: Charmonium family created by individual states. The invariant mass of quarkonium state and its quantum numbers determine the position of state in the picture. Invariant mass defines vertical position. Heavier states are in the top. The figure is taken from [51].

lision are directly produced. J/ψ can be also produced from a feed-down of B mesons. This is called a non-prompt production.

At first quarkonium discoveries of J/ψ and Υ are going to be discussed in this chapter. Afterwards, quarkonia as probes of the quark-gluon plasma creation will be discussed.

2.1 Discovery of J/ψ

Discovery of J/ψ was announced in 1974 [52] (page 57). Two groups, of S. Ting from BNL and B. Richter from SLAC, published papers on the discovery the same day. Particle was named J by the Ting's group and ψ by Richter's one, together J/ψ [52] (page 57). Both groups were awarded Nobel Prize for their pioneering work. At first we will discuss experiment from BNL.

Narrow and high peak in the cross section of the reaction $p + Be \rightarrow e^+ + e^- + X$ was observed. The J particle, as it was named by the Ting's group, had the mass around $3.1 \text{ GeV}c^{-2}$ and the width was surprisingly narrow. They measured the e^+e^- mass spectrum by a spectrometer with two arms [13]. In another words, they were searching for some particle that decays to a positron and electron pair. The invariant mass m_0 of this particle can be easily calculated from the knowledge of relativistic energy of positron E_+ and electron E_- and their momenta p_+ and p_- . For simplicity we will calculate m_0 in natural units ($c = 1$). We use the following convention:

$$\vec{p}c = \vec{P}, m_0c^2 = M \quad (2.1)$$

An equation can be rewritten as follows.

$$E^2 = m_0^2c^4 + \vec{p}^2c^2 = M^2 + \vec{P}^2 \quad (2.2)$$

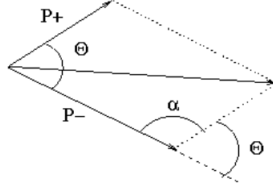


Figure 2.2: Momenta of an electron and a positron after the reaction $J/\psi \rightarrow e^+ + e^-$, Θ , the angle between the momenta and the angle α , the complementary angle to Θ . Figure is taken from [52].

If the particle decays to n others, the previous equation has the form

$$M^2 = E^2 - \vec{P}^2 = \left(\sum_i^n E_i \right)^2 - \left(\sum_i^n \vec{P}_i \right)^2. \quad (2.3)$$

In our example of decay to electron and positron we obtain following equations.

$$\begin{aligned} M^2 &= E^2 - \vec{P}^2 = (E_+ + E_-)^2 - (\vec{P}_+ + \vec{P}_-)^2 = \\ &= (E_+ + E_-)^2 - (P_+^2 + P_-^2 - 2P_+P_- \cos \alpha) = \\ &= (E_+ + E_-)^2 - (P_+^2 + P_-^2 + 2P_+P_- \cos \theta) \end{aligned} \quad (2.4)$$

The value of momentum of positron is denoted P_+ , momentum of electron P_- . α is the complementary angle to the angle between vectors of momenta of positron and electron. During expansions of \vec{P}^2 the law of cosines was used. Afterwards, identity $\cos \alpha = -\cos \theta$ was used, where θ is the angle between momenta. Situation can be seen in the Figure 2.2. Previous method is taken from [52] (page 82) and slightly modified.

Analogously, Ting's group calculated the invariant mass of observed particle. Their results are shown in the Figure 2.3. A narrow peak around $3.1 \text{ GeV}c^{-2}$ can be seen. Ting made many checks. In the picture are displayed results of the check connected to a magnet.

However, as was mentioned before Ting's group was not the only one that published an article about the J/ψ resonance. Richter's group from Stanford Linear Accelerator announced the observation of resonance with the mass around $3.1 \text{ GeV}c^{-2}$ as well as Ting's group. Richter's group collided electrons with positrons at different center-of-mass energies. At first they searched for particles which decays to hadrons [14]. The scan was performed by 200 MeV steps. 30% enhancement appeared at $3.2 \text{ GeV}c^{-2}$. It was caused by high energy tail as was proved after. Subsequently, they looked at $3.1 \text{ GeV}c^{-2}$ and $3.3 \text{ GeV}c^{-2}$ and noticed 3 to 5 higher cross section in 2 from 8 runs at $3.1 \text{ GeV}c^{-2}$ caused by narrow resonance. Finally, they scanned cross section of multihadron final

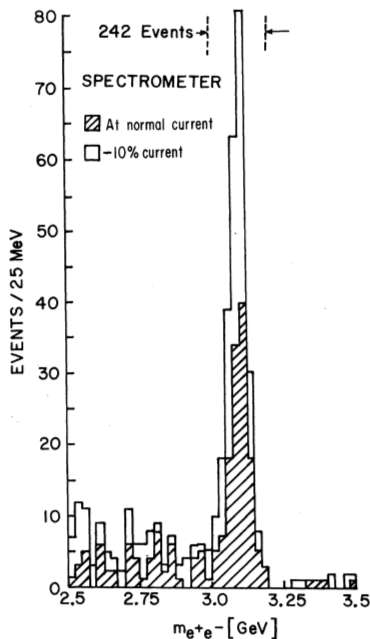


Figure 2.3: The results of BNL group. There is the calculated mass of particle J on x-axis and the number of events on y-axis. Shaded area corresponds to normal magnet setting and unshaded one to magnet setting about 10% lower than the normal one. The picture is taken from [56].

states, e^+e^- final states and $\mu^+\mu^-$, $\pi^+\pi^-$, K^+K^- together, using much finer energy steps, and observed resonance. They were not able to discriminate between $\mu^+\mu^-$, $\pi^+\pi^-$ and K^+K^- , because their muon identifications system did not function [14]. However, it is known today J/ψ decays to $\mu^+\mu^-$.

2.2 Discovery of Υ

Ledermans group discovered another heavy particle decaying in lepton-antilepton pair in 1977 in Fermilab laboratory [37]. They used a double-arm spectrometer such as the Tings group in the case of J/ψ discovery. They observed muons and antimuons from collisions of a proton with targets $p + (Cu, Pt) \rightarrow \mu^- + \mu^+$ anything [37]. The computation of invariant mass was similar to that of J/ψ .

The invariant mass dimuon spectrum was measured and significant enhancement in the region of $9 - 10 \text{ GeV}c^{-2}$ was observed [37].

The Fermilab group discussed the possible quark-antiquark composition of Υ in the other paper [36] and refers to the work of Gottfried and Eichstein in this paper. They mentioned that there might be three states with invariant masses close to each other and calculated "distances" between peaks on the base

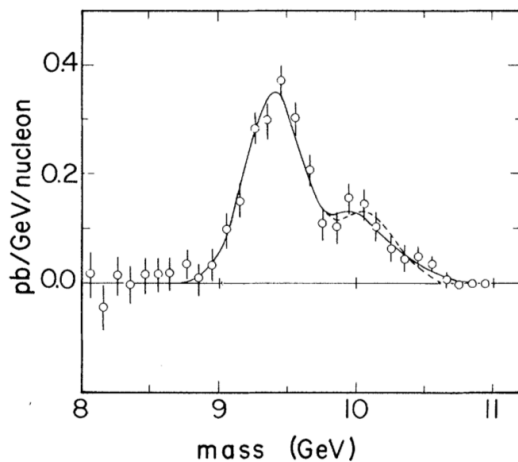


Table 2.4: Excess of data over continuum fit from paper [36]. The solid curve marks three-peak fit, the dashed curve two-peak fit. The picture is taken from [36].

of a theoretical potential between quark and antiquark [36]. Comparison of "distances" between peaks from Ledermans experiment and Eichstein-Gottfried predictions can be seen in 2.1.

Possible existence of the mentioned three Υ states was verified later. The invariant masses of $\Upsilon(1S)$, $\Upsilon(2S)$ and $\Upsilon(3S)$ are approximately $9.5 \text{ GeV}c^{-2}$, $10.0 \text{ GeV}c^{-2}$ and $10.4 \text{ GeV}c^{-2}$ [50].

		$\Delta m(\Upsilon' - \Upsilon)[MeV]$	$\Delta m(\Upsilon'' - \Upsilon)[MeV]$
Lederman experiment	Two-peak fit	650 ± 30	
	Three-peak fit	610 ± 40	1000 ± 120
Eichten and Gottfried	Three peaks	420	750

Table 2.1: The comparison of "distances" between peaks from the Ledermans experiment and the Eichstein-Gottfried predictions from [36].

2.3 Quarkona as the probes of a hot and dense medium in heavy-ion collisions

Heavy quarks are produced during the hard-scattering initial stage of heavy-ion collisions. Subsequently, heavy quarks whether deconfined or bounded in hadrons can be affected by occurring stages of a matter. Thus, we can learn more about properties of the created medium by looking at modifications

of heavy flavour hadron production. Additionally, heavy quarks are unique probes of the strongly interacting matter in heavy-ion collisions, since they interact with the medium differently from light quarks [58].

Quarkonia can be used as probes of QGP. It was suggested that extremely hot and dense matter in the form of the quark-gluon plasma may occur in more central and energetic heavy-ion collisions and the quark-antiquark potential can be Debye-like screened by the medium [58]. Debye-screening radius decreases with temperature. If Debye radius is smaller than the radius of quarkonium, quark and its antiquark can be separated and quarkonium is "melted" in the medium [47]. Yields of quarkonia per binary nucleon-nucleon collision may be reduced by this phenomenon in the comparison to pp collisions. The "melting" of quarkonia is sequential and reflects the binding energy of quarkonium [48]. Thus, quarkonia can be used as "thermometer" of the matter. See the Figure 2.5.

The dissociation of a quark-antiquark pair is expected to depend on a temperature of the deconfined matter [25]. This dependence is illustrated by the cartoon in the Figure 2.5. For example $\Upsilon(nS)$ states might be useful for studying the medium temperature.

The physical quantity that can be measured and provides comparison to the pp collisions is called nuclear modification factor R_{AA} . It is invariant cross section per p_T bin or bin of another quantity obtained from collision dN^{AA}/dp_T scaled to invariant mass from pp collisions dN^{pp}/dp_T . There is one possible definition [53]

$$R_{AA}(p_T) = \frac{dN^{AA}(p_T)/dp_T}{\langle N_{coll}(p_T) \rangle \frac{dN^{pp}}{dp_T}}, \quad (2.5)$$

where $\langle N_{coll} \rangle$ is a number of binary collisions. If the collision is only the superposition of binary collisions, R_{AA} would be equal to one. If the yield is suppressed, R_{AA} is smaller than one.

The suppression of $\Upsilon(nS)$ states was studied by the CMS Experiment at CERN. Results from $PbPb$ and pp collisions at the center-of-mass energy per nucleon pair 2.76 TeV was presented in [25]. The results are depicted in the Figure 2.6. As can be seen on the left side of the Figure 2.6, the ratio of $\Upsilon(2S)$ to $\Upsilon(1S)$ yields in $PbPb$ collisions is lower in comparison to the same ratio in pp collisions at all measured centrality bins. The yields of $\Upsilon(1S)$ are suppressed in the comparison to pp collisions from the second centrality bin as can be seen on the right of Figure 2.6 with $R_{AA}(N_{part})$. N_{part} is a number of participants of a collision. If the N_{part} rises, the collision is more central. There are depicted R_{AA} of $\Upsilon(1S)$ and $\Upsilon(2S)$ from $PbPb$ collisions from the CMS in the Figure 2.6. Data exhibit decreasing trend with increasing N_{part} . $\Upsilon(2S)$ states are significantly more suppressed than $\Upsilon(1S)$ states at all centralities. It can be seen also on the left panel of 2.6, where the dependence of the double ratio on the number of participants can be seen.

The data favour the scenario of a stronger suppression of excited Υ states [25]. However, measured modification of yields cannot be attributed only to "melt-

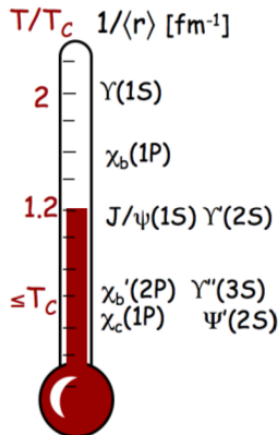


Figure 2.5: The cartoon illustrating the ”temperatures of quarkonia melting”. The picture is taken from [48].

ing” of $\Upsilon(nS)$. There are other phenomena altering quarkonium yields. For example the feed-down contribution of excited states. Furthermore, cold-nuclear-matter effects are needed to be taken into account.

2.4 Other effects altering quarkonia yields

As was mentioned earlier, yields of quarkonia may be altered by various phenomena occurring during the collisions [59]. Quark and antiquark may create bound state also during different stages of heavy-ion collisions, for example during evolution of hot and dense medium or hadronization. This phenomenon is called (re)combination and causes enhancement of quarkonium yields.

Cold nuclear matter effects such as alteration of parton distribution functions in nucleons, nuclear absorption or absorption on a comoving hadron may be also significant. If a nucleon is bounded in nuclei, parton distribution function differs from a distribution function of a free nucleon. It causes differences between probability of $q\bar{q}$ -pair formation. The second mentioned phenomenon, nuclear absorption, is especially relevant for heavy-ion collisions at lower center-of-mass energies and collisions of nucleon with heavy ion, since $q\bar{q}$ pair can be created while traversing nuclei. $q\bar{q}$ pairs can be also affected by comoving hadrons. Moreover, $q\bar{q}$ pairs can lose energy due to interaction with medium. Thus, its momentum could be decreased and quarkonium yields per higher p_T bins could be lower, whereas yields per lower p_T bins could be enhanced.

It is challenging to distinguish between these phenomena and explain the altering of yields in comparison to pp collisions precisely. There are many models available on the market that can be compared to experimental data.

For example, measurements of the J/ψ nuclear modification factor at $\sqrt{s_{NN}} =$

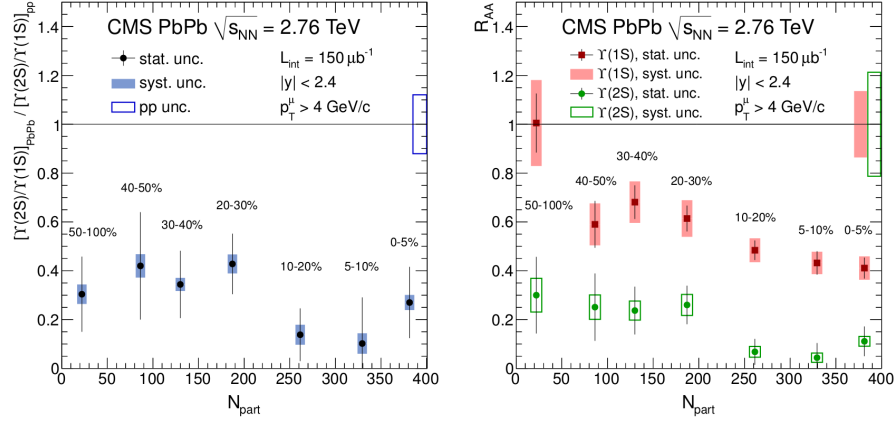


Figure 2.6: The dependance of the double ratio on the number of participants N_{part} on the left. The nuclear modification factor R_{AA} is shown on the right. Event centrality bins are specified by centrality percentages. The picture is taken from [25].

200 GeV were performed by PHENIX and STAR experiments [59]. Figure 2.7 shows obtained R_{AA} as a function of centrality, for different p_T ranges. The results are compared to two model predictions, Zhao and Rapp [61] and Liu et al. [44], which take into account J/ψ suppression due to the color screening, as well as recombination as cold nuclear matter effects. Strong suppression is observed for low p_T J/ψ in all centrality bins. Also, high- p_T J/ψ are suppressed in central collisions, what suggests QGP formation.

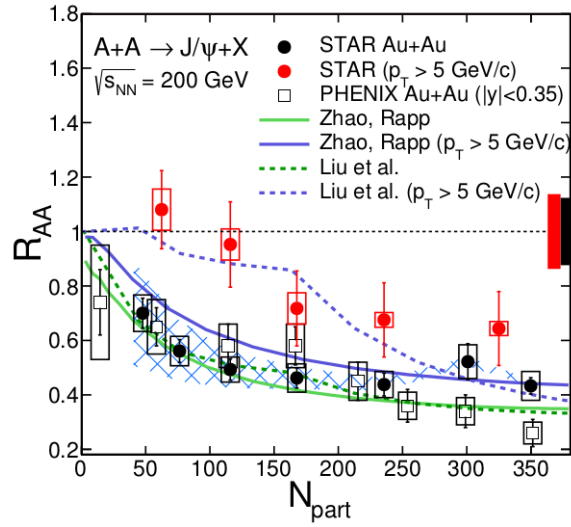


Figure 2.7: J/ψ R_{AA} as function of a number of participants N_{part} compared to different model predictions. The data from AuAu collisions at $\sqrt{s_{NN}} = 200 \text{ GeV}$ and mid-rapidity were measured by the PHENIX and the STAR. The low- p_T ($< 5 \text{ GeVc}^{-1}$) STAR results from the STAR are marked by the red full circles, whereas the high- p_T ($> 5 \text{ GeVc}^{-1}$) STAR data are shown as the black full circles. The PHENIX measurements are marked with empty squares. The full lines corresponds to Zhao and Rapp predictions [61], whereas dashed to Liu et al. all predictions [44]. Green lines show predictions for low- p_T and blue lines for high p_T . The picture is taken from [59].

Chapter 3

Quarkonium production mechanism

There are three basic momentum scales in the case of quarkonium, quark mass m_Q , the momentum of the heavy quark or antiquark in the quarkonium rest frame (order of $m_Q c^2$), the binding energy of the quark-antiquark pair (order of $m_Q v^2$) [18]. v is the typical velocity of the heavy quark in the quarkonium rest frame. For charmonium $v_c^2 \simeq 0.23$ c and for bottomium $v_b^2 \simeq 0.08$ c [41]. A quarkonium production mechanism can be divided to two significantly different parts, the production of a heavy quark pair $q\bar{q}$ and the evolution to the bound quarkonium state [57]. $q\bar{q}$ in the hard scattering at the early stage of a collision. Significant momentum transfer is typical for this process, since at least energy equal to the mass of heavy $q\bar{q}$ is needed to be released. Therefore, the perturbative calculations can be used for the description of $q\bar{q}$ formation. The hadronization process follows. Lower momenta of order $m_Q v$ and $m_Q v^2$ are transferred [18]. The non-perturbative approach has to be used for the calculations connected to the hadronization process. The separation of perturbative (typical for short distances) and non-perturbative processes (typical for long distances) is called factorization. There are many theoretical attempts that try to describe the dynamical the evolution of the $q\bar{q}$ pair, for example colour-evaporation model (CEM), the colour-singlet model (CSM), the non-relativistic QCD (NRQCD) factorization approach with colour-octet contributions in addition to the colour singlet.

3.1 The colour-evaporation model (CEM)

The CEM is built on the assumption that every $q\bar{q}$ pair with mass smaller than that of the lightest open-heavy-flavour meson (H) pair and higher than invariant mass of a heavy quark and its antiquark evolve into a quarkonium [18]. Quantum numbers of $q\bar{q}$ such as colour and total angular momentum with its alignment are randomized. The non-perturbative probability F_Q of that $q\bar{q}$ pair

evolving into a heavy quarkonium state Q is expected to be process independent. There are nine possible colour combinations for $q\bar{q}$, but there is only one colour-singlet combination. There are $2J_Q + 1$ possible eigenstates of the operator J_z and $\sum_i (2J_i + 1)$, where i runs over possible quarkonium states with mass under the mass of open-flavour heavy meson pair. Therefore, we can calculate probability F_Q as follows [10]

$$F_Q = \frac{1}{9} \frac{2J_Q + 1}{\sum_i (2J_i + 1)}. \quad (3.1)$$

We can count the total cross section of the quarkonium production as [10]

$$\sigma_Q = F_Q \int_{2m_q}^{2m_H} \frac{d\sigma_{q\bar{q}}}{dm_{q\bar{q}}} dm_{q\bar{q}}, \quad (3.2)$$

where $2m_H$ is the invariant mass of an open-heavy-flavour meson pair and $2m_q$ is the invariant mass of $q\bar{q}$ pair.

Within the CEM, the cross section for a specific quarkonium state, for example $J\psi$, is calculated by formula [41]

$$\sigma_{J/\psi} = \varrho_{J/\psi} \sigma_Q, \quad (3.3)$$

where $\varrho_{J/\psi}$ is the inverse of number of quarkonium lying between $2m_c$ and $2m_D$. $2m_D$ is determined from the fit to the data.

Quantum numbers are randomized, thus the CEM does not have the predictive power for polarization of quarkonia.

3.2 The colour-singlet model (CSM)

The CSM is established on assumptions different from that of the CEM. The quantum numbers such as spin are the same from the creation of $q\bar{q}$ pair to the hadronisation, because the gluon emissions are suppressed [10]. Only the $q\bar{q}$ pairs in the colour-singlet state evolve into quarkonium. The CS model is based on expansion in α_s . The first power of α_s that is not equal to zero is called leading order (LO).

$q\bar{q}$ are produced for example through a gluon fusion. The reactions contributing to the production of quarkonia within the LO CSM can be seen in the Figure 3.1.

The $q\bar{q}$ pair may evolve into a quarkonium. Only $q\bar{q}$ pairs in the colour-singlet state with the same spin and angular-momentum quantum numbers as a certain quarkonium state develops into this quarkonium [18].

3.3 The non-relativistic quantum chromodynamics (NRQCD) approach

The NRQCD is the effective field theory. In this theory, $q\bar{q}$ pairs in the colour-singlet and the colour-octet state may develop into a final color-singlet quarko-

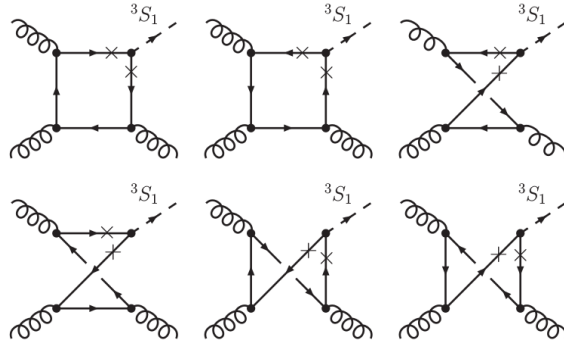


Figure 3.1: The Feynman diagrams for $qq \rightarrow {}^3S_1 g$ reactions, which contribute to the quarkonium production within the LO CSM. Figure is taken from [41].

onium state. A resulting meson is colourless, however $q\bar{q}$ pair can be transformed to colour-singlet state by emission of a low-energy gluon [57].

Important feature of the NRQCD is factorization. Calculations are divided to the short-distance perturbative part, long-distance non-perturbative calculations connected to the hadronization of the $q\bar{q}$ pair. According to NRQCD, the hadronization part of the process is described by non-perturbative long-distance matrix elements (LDME) [57]. The colour-singlet contribution to LDME is calculated within the model, whereas the colour-octet with transition to colour-singlet state contribution are not determined within the theory. These elements are determined by a fit to an experimental data.

The theory is based on expansion in α_s and v [57]. The first powers of α_s and v that are not equal to zero are called leading order (LO). Further, we can expand to the higher orders, next-to-leading order (NLO), next-to-next-to-leading order (NNLO) etc.

There are different models that are trying to describe the quarkonium production mechanism, for example k_T -factorization [35], TMD factorisation [17] and the combined use of the CGC formalism [38] and NRQCD [10].

All mentioned models predict cross section for quarkonium production. Some of the predictions can be seen in the Figure 3.2.

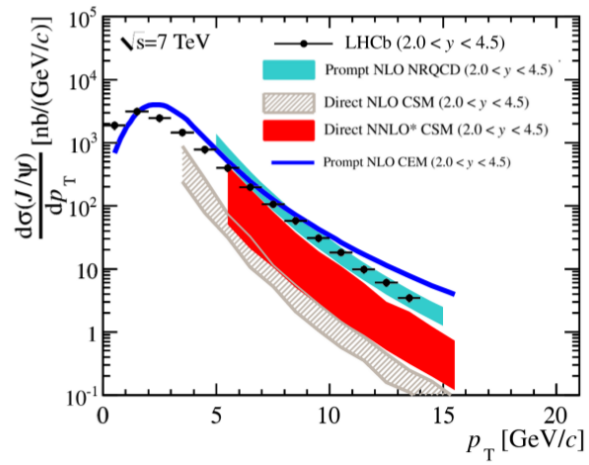


Figure 3.2: Prompt J/ψ yield as measured by LHCb ([3]) at $s = 7$ TeV compared to different theory predictions, prompt NLO NRQCD ([45]), direct NLOCS ([20], [11]) direct NNLO CS ([12], [42]) and prompt NLO CEM ([32]). Figure is taken from [10].

Chapter 4

The Polarization of Quarkonia

Quarkonia can be produced by the superposition of processes. These processes may define subset of possible eigenstates of the angular momentum component J_z , where z is suitably chosen quantization axis. We call this phenomenon the quarkonium polarization [31].

There are many theoretical approaches to describe the production mechanism of quarkonia and they imply different predictions of the polarization. Thus, the polarization of quarkonia may play the key role in distinguishing between them. However, current results are not sufficient for this purpose and some of them seem to be contradictory [30]. More appropriate measurements, systematic and various approaches to the polarization are needed to be performed before conclusions. Basic concept of the quarkonium polarization will be discussed in this chapter.

We will focus on vector quarkonium polarization in this thesis. The vector meson is designation for meson with quantum numbers $J^{PC} = 1^{--}$. The concept of these mesons' polarization is similar to polarization of photon, because both of them have the same charge-parity. If the z component of the total angular momentum is equal to ± 1 , we say the quarkonium has transverse polarization. In the case of $J_z = 0$ quarkonium has longitudinal polarization.

The lepton-antilepton pair is also characterized by the same charge-parity. Therefore, vector quarkonium, such as J/ψ , ψ' and $\Upsilon(nS)$ states, can decay in a lepton-antilepton pair. A lepton and an antilepton are created with the same-sized opposite momenta in the quarkonium rest frame thanks to momentum conservation law. The probability distribution of quarkonium dilepton decay corresponds to the polarization of quarkonium [31]. Anisotropic distribution indicates polarization of measured quarkonia, whereas spherically symmetric distribution implies that quarkonia are unpolarized. The graphical dilepton decay distribution of transversely and longitudinally polarized quarkonia in a natural frame can be seen in the Figure 4.1. The natural frame is the frame in which

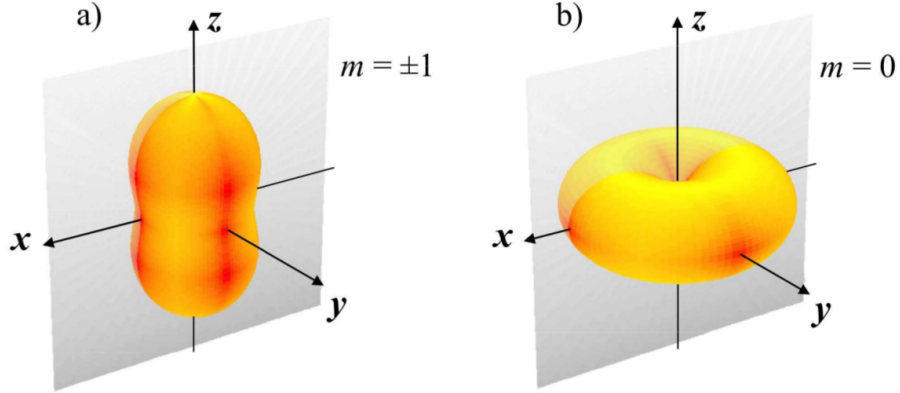


Figure 4.1: The graphical representation of the dilepton decay distribution of a) "transversely" and b) "longitudinally" polarized quarkonia. m is the magnetic quantum number of a quarkonium. The picture is taken from [31].

there is no the azimuthal anisotropy (polar and azimuthal angles will be discuss later).

4.1 Reference Frames

If we want to measure quarkonium polarization, we need to define suitable reference frame. The plane containing both beams and the direction of the flight of a quarkonium is called the production plane. This definition can be seen on the left panel of the Figure 4.3 on the left. The xz plane is defined identically with the production plane in the case of the inclusive production, which we consider. y -axis is perpendicular to the production plane and together with x -axis and z -axis constitutes the right-handed coordinate system. Subsequently, the determination of z -axis (determination of its direction and the origin of the coordinate system lying on it) is sufficient for an unambiguous definition of a frame. Further, the angles ϑ and φ can be determined by the direction of the flight of positively charged lepton. The polar angle ϑ is the angle between positron momentum and z -axis. The azimuthal angle φ is defined as the angle between x -axis and a positive-lepton momentum projection to the xy -plane. The definition of the angles can be seen in the Figure 4.2.

There are many possible conventions for the definition of z -axis, called a polarization axis. We will discuss here three reference frames, commonly used in experiments. In principle all these reference frames can be called quarkonium rest frame. First one is called Gottfried-Jackson frame. The orientation of z -axis is defined by the direction of one beam [31]. Within second frame, Collins-Soper frame, z -axis is determined as a bisector of the angle between the momentum of particles in one beam \vec{P}_1 and the minus momentum $-\vec{P}_2$ of particles [31].

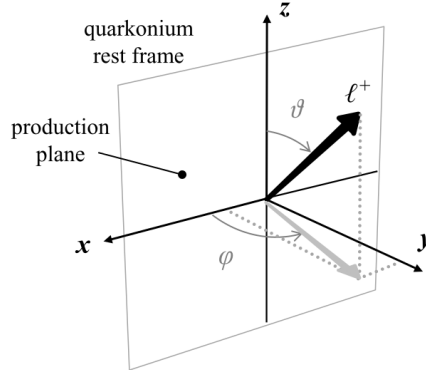


Figure 4.2: The definition of angles ϑ and φ describing direction of flight of positive lepton from the quarkonium decay. The arrow marked by l^+ shows the direction. ϑ is defined as the angle between positron momentum and z-axis and φ as the angle between x-axis and a positive-lepton momentum projection to the xy-plane. The picture is taken from [31].

The direction of z-axis in this case can be expressed as follows [57]:

$$\vec{z} = \frac{\vec{P}_1}{|\vec{P}_1|} - \frac{\vec{P}_2}{|\vec{P}_2|}. \quad (4.1)$$

The situation is outlined in the Figure 4.3. Third reference frame abundantly used in experiments is called the center-of-mass helicity frame [31]. The direction of z-frame is defined by the direction of a quarkonium momentum in the center-of-mass frame.

4.2 Dilepton Decay Angular Distribution

As was mentioned, quarkonium may decay to a lepton and an antilepton. We can experimentally determine directions of flights of leptons and obtain dilepton decay angular distribution.

In this chapter we only consider the inclusive production, thus xz -plane merge with production plane containing vector meson and beams, because all possible experimentally definable polarization axes are situated in production plane [30]. If quarkonia in an experiment originate from n processes, the most general dilepton decay angular distribution can be written as

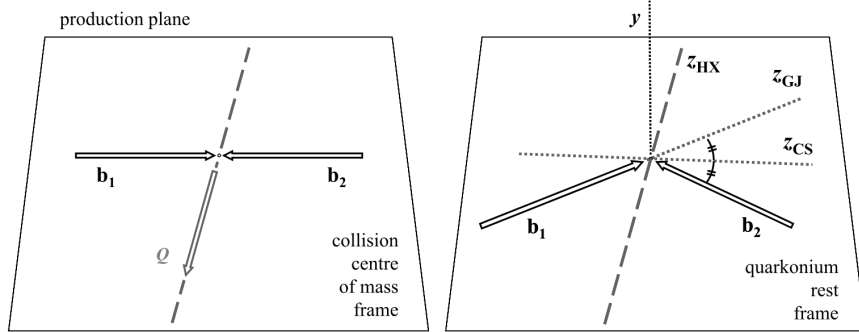


Figure 4.3: The definition of production plane on the left. and three commonly used coordinate systems on the right, Gottfried-Jackson (GJ) and Collins-Soper (CS), and the helicity frame (HX). The picture is taken from [31].

$$\begin{aligned}
 W(\cos \vartheta, \varphi) &= \sum_{i=1}^n f^{(i)} W^{(i)}(\cos \vartheta, \varphi) \propto \\
 &\propto \frac{1}{3 + \lambda_\vartheta} (1 + \lambda_\vartheta \cos^2 \vartheta + \lambda_\varphi \sin^2 \vartheta \cos 2\varphi + \lambda_{\vartheta\varphi} \sin 2\vartheta \cos \varphi),
 \end{aligned} \tag{4.2}$$

where $f^{(i)}$ is weight of i -th single subprocess, $W^{(i)}$ dilepton decay angular distribution of i -th elementary subprocess and $\lambda_\vartheta, \lambda_\varphi, \lambda_{\vartheta\varphi}$ are polarization parameters [31]. The derivation of the equation (4.2) can be seen in [31]. We are capable of measuring the shape parameters in experiments. If we integrate the equation (4.2) over either φ or $\cos \vartheta$, we obtain one-dimensional angular distribution.

$$\begin{aligned}
 W(\cos \vartheta) &= \int_0^{2\pi} \frac{1}{3 + \lambda_\vartheta} (1 + \lambda_\vartheta \cos^2 \vartheta + \lambda_\varphi \sin^2 \vartheta \cos 2\varphi + \lambda_{\vartheta\varphi} \sin 2\vartheta \cos \varphi) d\varphi = \\
 &= \frac{1}{3 + \lambda_\vartheta} (1 + \lambda_\vartheta \cos^2 \vartheta)
 \end{aligned} \tag{4.3}$$

Both $\cos 2\varphi$ and $\cos \varphi$ vanish during integration over $[0, 2\pi]$.

$$\begin{aligned}
W(\varphi) &= \int_{-1}^1 \frac{1}{3 + \lambda_\vartheta} (1 + \lambda_\vartheta \cos^2 \vartheta + \lambda_\varphi \sin^2 \vartheta \cos 2\varphi + \lambda_{\vartheta\varphi} \sin 2\vartheta \cos \varphi) d \cos \vartheta = \\
&= \int_{-1}^1 \frac{1}{3 + \lambda_\vartheta} (1 + \lambda_\vartheta \cos^2 \vartheta + \lambda_\varphi (1 - \cos^2 \vartheta) \cos 2\varphi + 2\lambda_{\vartheta\varphi} (\sqrt{1 - \cos^2 \vartheta}) \cos \vartheta \cdot \\
&\cdot \cos \varphi) d \cos \vartheta = \int_{-1}^1 \frac{1}{3 + \lambda_\vartheta} (1 + \lambda_\vartheta x^2 + \lambda_\varphi (1 - x^2) \cos 2\varphi + 2\lambda_{\vartheta\varphi} \sqrt{1 - x^2} x \cdot \\
&\cdot \cos \varphi) dx = \frac{1}{3 + \lambda_\vartheta} \left[x + \lambda_\vartheta \frac{1}{3} x^3 + \lambda_\varphi \left(x - \frac{1}{3} x^3 \right) \cos 2\varphi \right]_{-1}^1 = \\
&= \frac{2}{3} \left(1 + \frac{2\lambda_\varphi}{3 + \lambda_\vartheta} \cos 2\varphi \right)
\end{aligned} \tag{4.4}$$

We used formulas $\sin^2 \vartheta = 1 - \cos^2 \vartheta$ and $\sin 2\vartheta = \sqrt{1 - \cos^2 \vartheta} \cos \vartheta$ valid at interval $[0, \pi]$. $f(x) = \sqrt{1 - x^2} x$ is odd function at interval $[-1, 1]$, thus this part vanishes during integration. Overall, we can write

$$W(\cos \vartheta) \propto \frac{1}{3 + \lambda_\vartheta} (1 + \lambda_\vartheta \cos^2 \vartheta), W(\varphi) \propto 1 + \frac{2\lambda_\varphi}{3 + \lambda_\vartheta} \cos 2\varphi. \tag{4.5}$$

Formulas (4.5) can be useful for separate determination of λ_ϑ and λ_φ . This method is helpful in cases of low-statistics analysis, since it may improve stability of a fit [31]. However, parameter $\lambda_{\vartheta\varphi}$ vanishes during both integrations. One of possible ways of gaining parameter $\lambda_{\vartheta\varphi}$ is defining of new variable $\tilde{\varphi}$ as

$$\tilde{\varphi} = \begin{cases} \varphi - \frac{3}{4}\pi & \text{for } \cos \vartheta < 0, \\ \varphi - \frac{1}{4}\pi & \text{for } \cos \vartheta > 0 \end{cases} \tag{4.6}$$

and obtaining the distribution

$$W(\tilde{\varphi}) \propto 1 + \frac{\sqrt{2}\lambda_{\vartheta\varphi}}{3 + \lambda_\vartheta} \cos \tilde{\varphi}, \tag{4.7}$$

as is written in [31].

Example of one dimensional $\cos \vartheta$ and φ distributions measured by the ALICE experiment are shown in the Figure (4.4), in the HX and the CS frames. J/ψ yield in each $\cos \vartheta$ or φ bin is obtained by the fitting dimuon invariant mass spectrum as shown in the Figure (4.5).

4.2.1 The Frame-Invariant Approach

Polarization axes are situated in the production plane in all here mentioned reference frames. Thus, we can rotate one reference frame about y -axis and obtain another by this way. A matrices corresponding to the rotation reference frame around y -axis by an angle δ and back are

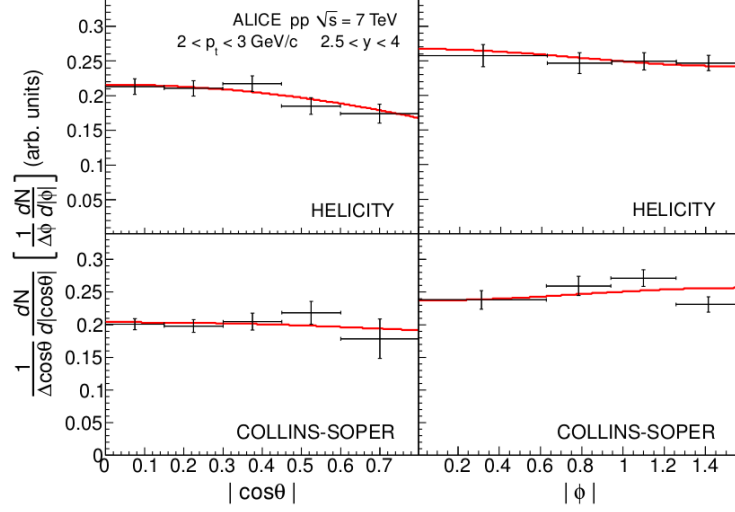


Figure 4.4: The acceptance-corrected angular distribution for the J/ψ decays muons, for $2 < p_T < 3 \text{ GeVc}^{-1}$. The distribution is simultaneously fitted by equations 4.5. The picture is taken from [5].

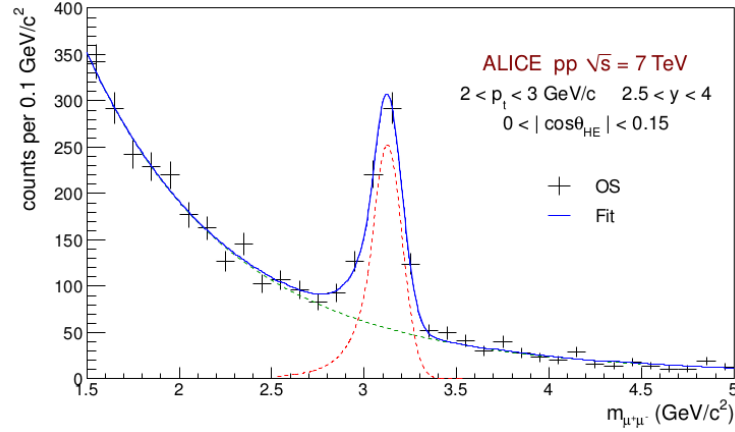


Figure 4.5: The dimuon invariant mass spectrum for $2 < p_T < 3 \text{ GeVc}^{-1}$, $0 < |\cos \vartheta| < 0.15$, together with the result of the fit. The J/ψ signal was described by a Crystal Ball (CB) function and background by an empirical function. The picture is taken from [5].

$$R_y(\delta) = \begin{pmatrix} \cos \delta & 0 & -\sin \delta \\ 0 & 1 & 0 \\ \sin \delta & 0 & \cos \delta \end{pmatrix}, R_y^{-1}(\delta) = \begin{pmatrix} \cos \delta & 0 & \sin \delta \\ 0 & 1 & 0 \\ -\sin \delta & 0 & \cos \delta \end{pmatrix}. \quad (4.8)$$

Therefore, the formula for the retrograde rotation of the unit vector in the spherical coordinates $\vec{r}' = (\sin \vartheta' \cos \varphi', \sin \vartheta' \sin \varphi', \cos \vartheta')^T$ in the rotated frame can be written as

$$\begin{aligned} \vec{r} &= R_y^{-1}(\delta) \vec{r}' = \begin{pmatrix} \cos \delta & 0 & \sin \delta \\ 0 & 1 & 0 \\ -\sin \delta & 0 & \cos \delta \end{pmatrix} \begin{pmatrix} \sin \vartheta' \cos \varphi' \\ \sin \vartheta' \sin \varphi' \\ \cos \vartheta' \end{pmatrix} = \\ &= \begin{pmatrix} \cos \delta \sin \vartheta' \cos \varphi' + \sin \delta \cos \vartheta' \\ \sin \vartheta' \sin \varphi' \\ -\sin \delta \sin \vartheta' \cos \varphi' + \cos \delta \cos \vartheta' \end{pmatrix} = \begin{pmatrix} \sin \vartheta \cos \varphi \\ \sin \vartheta \sin \varphi \\ \cos \vartheta \end{pmatrix}. \end{aligned} \quad (4.9)$$

If we substitute $\sin \vartheta \cos \varphi$, $\sin \vartheta \sin \varphi$ and $\cos \vartheta$ in the formula (4.2) by the expressions with the variables in the rotated frames from (4.9), we obtain

$$W(\cos \vartheta', \varphi') \propto \frac{1}{3 + \lambda'_\vartheta} (1 + \lambda'_\vartheta \cos^2 \vartheta' + \lambda'_\varphi \sin^2 \vartheta' \cos 2\varphi' + \lambda'_{\vartheta\varphi} \sin 2\vartheta' \cos \varphi'), \quad (4.10)$$

where

$$\lambda'_\vartheta = \frac{\lambda_\vartheta - 3\Lambda}{1 + \Lambda}, \lambda'_\varphi = \frac{\lambda_\varphi + \Lambda}{1 + \Lambda}, \lambda'_{\vartheta\varphi} = \frac{\lambda_{\vartheta\varphi} \cos 2\delta - \frac{1}{2}(\lambda_\vartheta - \lambda_\varphi) \sin 2\delta}{1 + \Lambda}, \quad (4.11)$$

$$\text{with } \Lambda = \frac{1}{2}(\lambda_\vartheta - \lambda_\varphi) \sin^2 \delta - \frac{1}{2}\lambda_{\vartheta\varphi} \sin 2\delta,$$

as is written in [31].

Frame-independent inequalities for the parameters can be derived from another conditions [31].

$$|\lambda_\vartheta| \leq 1, |\lambda_\varphi| \leq \frac{1}{2}(1 + \lambda_\vartheta), \quad (4.12)$$

$$|\lambda_\varphi| \leq 1, |\lambda_{\vartheta\varphi}| \leq \frac{1}{2}(1 - \lambda_\varphi), \text{ for } \lambda_\varphi \leq -\frac{1}{3}: (2\lambda_\varphi + 1)^2 + 2\lambda_{\vartheta\varphi}^2 \leq 1. \quad (4.13)$$

Allowed regions for the decay angular parameters λ_φ depending on λ_ϑ and $\lambda_{\vartheta\varphi}$ depending on λ_φ following from inequalities (4.12) and (4.13) are shown in the Figure 4.6.

The choice of suitable reference frame is important, because for example fully "transverse polarization" in natural frame after the rotation $\delta = 90^\circ$ is not fully "longitudinal polarization". In the other words, the decay angular parameters

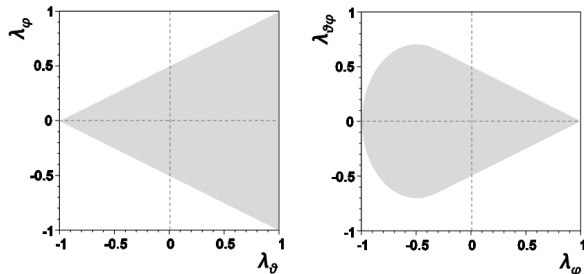


Figure 4.6: Allowed regions for parameters λ_θ depending on λ_φ and $\lambda_{\theta\varphi}$ depending on λ_φ shaded by grey colour. Left picture corresponds to inequalities (4.12), right to (4.13). Figure is taken from [31].

in the natural frame $\lambda_\theta = +1$ and $\lambda_\varphi = 0$ can be transformed by the rotation $\delta = 90^\circ$ to $\lambda'_\theta = \frac{1}{3}$, $\lambda'_\varphi = -\frac{1}{3}$ as can be seen in the Figure 4.7. A rotation angle between the helicity frame and Collins-Soper or Gottfried-Jackson frame depends on a longitudinal momentum p_L and a transverse momentum p_T of a quarkonium. Thus, if quarkonia are, for example, "transversely" polarised in the helicity frame, polarization parameters in Collins-Soper frame are dependent on p_T and p_L . Moreover, an acceptance of detectors can strongly affect such data analysis. Overall, trends simple in one reference frame may be alter by a change of reference frame to not so clearly interpretable trends and searching for physical explanation may be more difficult.

As was mentioned above, interpretation of results may be less complicated, if we use suitable reference frame. The frame invariant approach can help us with comparing results obtained in different reference frames and draw frame-independent conclusions.

The transformation properties (4.11) of (4.2) imply the existence of an frame invariant

$$F_{(c_1, c_2, c_3)} = \frac{(3 + \lambda_\theta) + c_1(1 - \lambda_\varphi)}{c_2(3 + \lambda_\varphi) + c_3(1 - \lambda_\varphi)}, \quad (4.14)$$

where c_1, c_2, c_3 are definite real parameters. The invariant has the same value for the same data in all reference frames. One possible combination of the parameters is $c_1 = -3, c_2 = 0, c_3 = 1$ [31]. Corresponding rotational invariant has the shape

$$\tilde{\lambda} = F_{(-3, 0, 1)} = \frac{\lambda_\theta + 3\lambda_\varphi}{1 - \lambda_\varphi}. \quad (4.15)$$

The possible decay angular distributions for $\tilde{\lambda} = 1$ and $\tilde{\lambda} = -1$ are shown in the Figure 4.7. $\tilde{\lambda} = 1$ corresponds to the transverse polarization and $\tilde{\lambda} = -1$ to the longitudinal polarization.

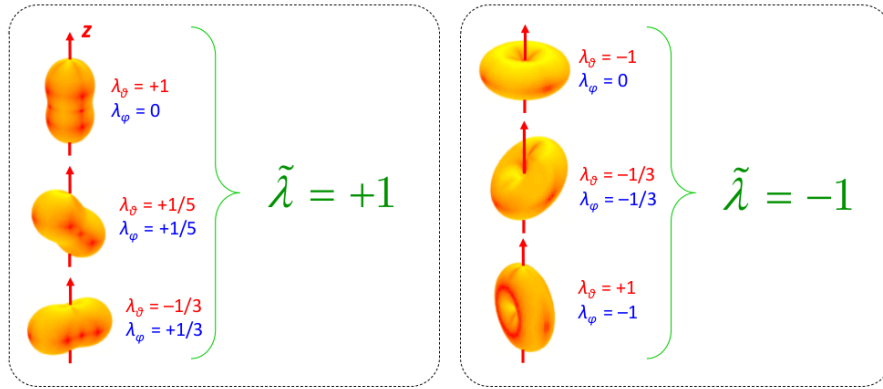


Figure 4.7: The rotations of graphical representation of the total angular dilepton decay distribution corresponding to transverse and longitudinal polarization and values of parameters λ_φ , λ_θ and the frame invariant from (4.15). The case of transverse polarization with invariant $\tilde{\lambda} = 1$ is on the left, "longitudinal" case with $\tilde{\lambda} = -1$ on the right. The Figure is taken from [29].

Chapter 5

Measurements of quarkonium polarization in proton-proton and proton-antiproton collisions

5.1 J/ψ polarization measurements in pp collisions at $\sqrt{s} = 200$ GeV by the STAR and PHENIX experiments

The PHENIX experiment at RHIC reported the J/ψ polarization measurements in pp collisions in the dielectron decay channel at $\sqrt{s} = 200$ GeV [9]. They performed measurements of inclusive J/ψ with $p_T < 5$ GeV c^{-1} at the mid-rapidity region $|y| < 0.35$. Direct J/ψ and J/ψ from feed-down from heavier charmonium states and B mesons are included in results. The angular dilepton distribution integrated over azimuthal angle φ was reconstructed for the purpose of gaining the polarization parameter λ_θ .

The STAR experiment also reported measurements of inclusive J/ψ polarization in pp collisions at $\sqrt{s} = 200$ GeV [8], via the dielectron decay channel. The polarization parameter λ_θ was reconstructed via the angular dilepton distribution integrated over azimuthal angle φ , as in the case of the PHENIX measurements. The rapidity region was broader, $|y| < 1$, and the explored p_T region was $2 < p_T < 6$ GeV c^{-1} .

In the PHENIX experiment, the parameter λ_θ was studied as a function of p_T in the HX, CS and GJ frames. The STAR experiment published results only for the HX frame vs. p_T . λ_θ was obtained in each reference frame by the fitting measured and subsequently corrected $\cos\theta$ distributions by the following

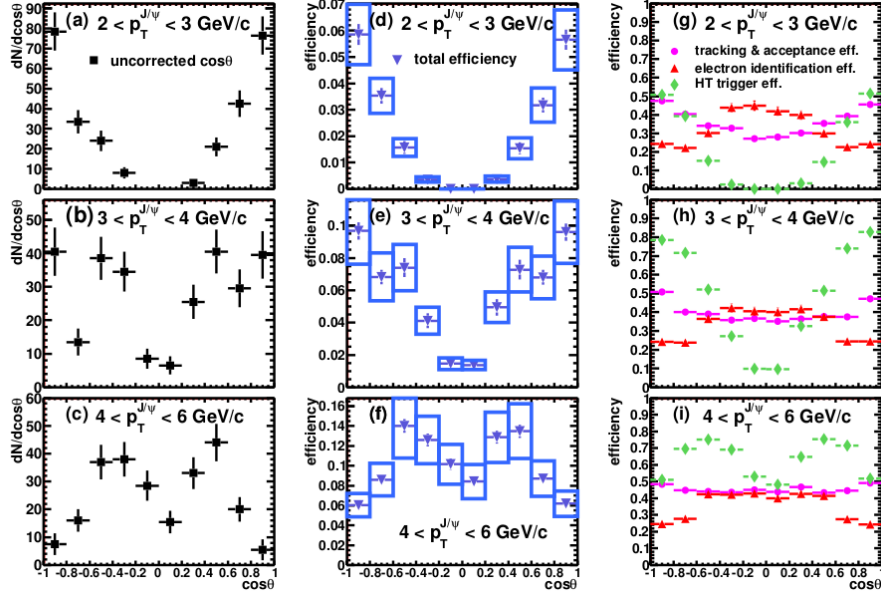


Figure 5.1: Panels (a)-(c) show uncorrected $\cos\vartheta$ distributions after the combinatorial background subtraction, for each p_T bin. Panels (d)-(f) show total efficiencies as function of $\cos\vartheta$. Systematics errors are shown as boxes. Panels (g)-(i) show different efficiencies that contribute to the total efficiency. The figure is taken from [8].

function

$$f(\cos\vartheta) = A(1 + \lambda_\vartheta \cos^2\vartheta). \quad (5.1)$$

Example of uncorrected $\cos\vartheta$ distributions after the combinatorial background subtraction and efficiencies from the STAR experiment are shown in the Figure 5.1. Corrected for the efficiency, fitted $\cos\vartheta$ distributions are presented in the Figure 5.2.

The fitting was performed in three p_T bins. In the case of the PHENIX experiment, it was $0 < p_T < 1$ GeV c^{-1} for the first bin, $1 < p_T < 2$ GeV c^{-1} for second one, and $2 < p_T < 5$ GeV c^{-1} . In the STAR case, measured p_T region was divided to intervals $2 < p_T < 3$ GeV c^{-1} , $3 < p_T < 4$ GeV c^{-1} and $4 < p_T < 6$ GeV c^{-1} .

The λ_ϑ parameter measured by PHENIX in the CS frame was out of the physically relevant interval $[-1, 1]$. The resulting values of the parameter λ_ϑ in the HX from both experiments can be seen in the Figure 5.3. The parameter in the GJ frame is depicted in the Figure 5.4. In the case of the PHENIX experiment, the values of the λ_ϑ in the GJ frame are spread over a broader region than in the HX, but have similar trend vs. p_T .

The trend of the data in the HX frame are similar for both discussed experiments. The parameter λ_ϑ decreases with increasing p_T . Strong longitudinal

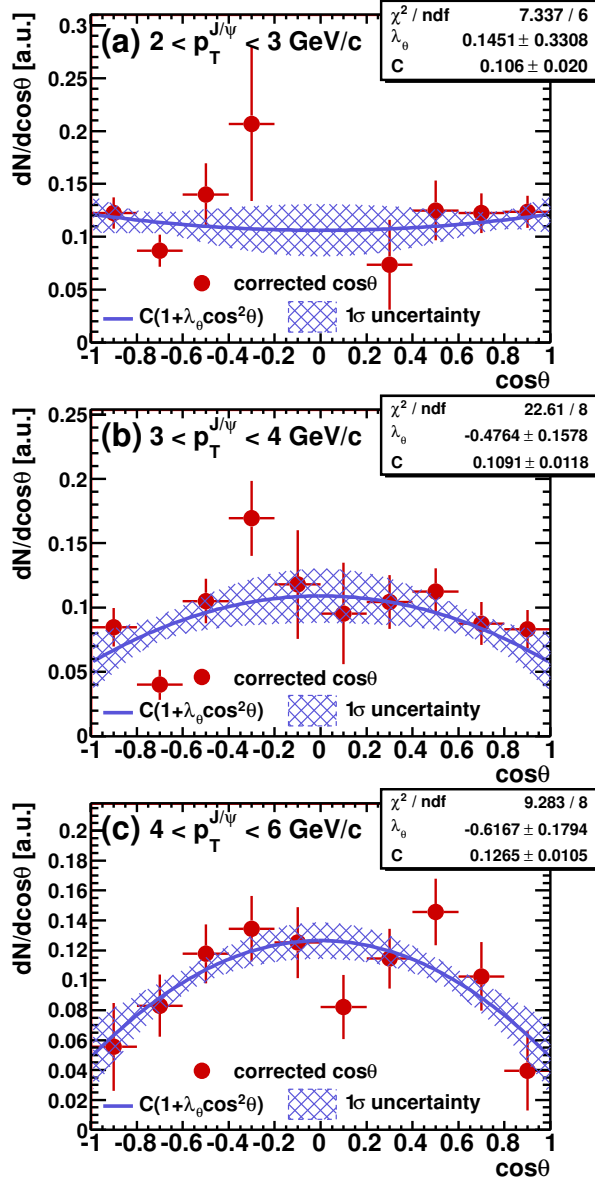


Figure 5.2: Corrected $\cos\vartheta$ distributions fitted with the function in equation (5.1). Blue line represents fit, the errors are statistical. Blue hatched area represents the 1σ uncertainty. The figure is taken from [8].

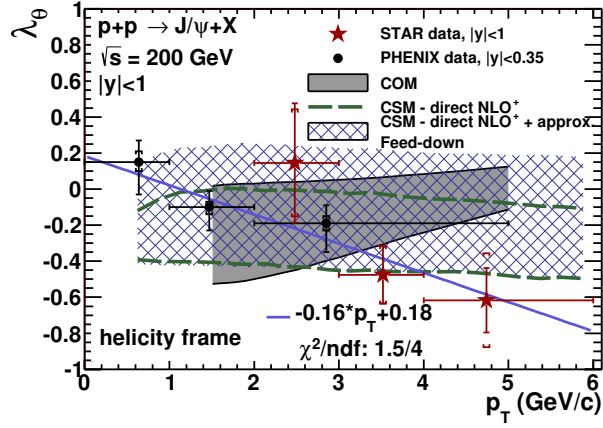


Figure 5.3: The polarization parameter λ_ϕ as the function of p_T in the HX frame. Red stars marks results of the STAR measurements, whereas black circles corresponds to the PHENIX measurements. The blue line is the fit of both sorts of the data. Statistical and systematic uncertainties are taken into the account. Data are compared to different model predictions. Green dashed lines demarcate NLO⁺ colour-singlet model (CSM) prediction for direct J/ψ . Hatched blue region is extrapolation for the prompt J/ψ . Gray shaded area represents LO NRQCD calculations with colour-octet contribution (COM). The horizontal errorbars denote the widths of p_T bins. The figure is taken from [8].

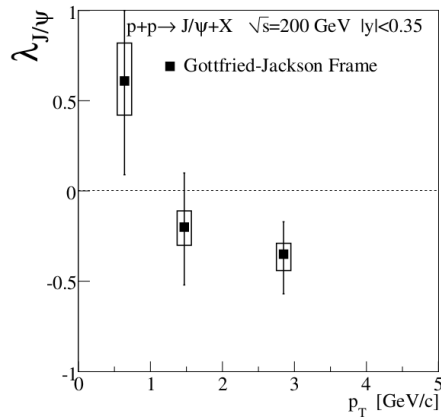


Figure 5.4: Results of the PHENIX experiment. The polarization parameter λ_ϕ marked as $\lambda_{J/\psi}$ as the function of p_T . The figure is taken from [9].

polarization can be observed for $p_T > 3 \text{ GeVc}^{-1}$ in the STAR experiment.

The data for the HX frame are compared to two model predictions, NLO⁺ CSM from [43] and LO COM from [27]. The LO COM (marked by the shaded area in the Figure 5.3) are predictions for direct J/ψ . The NLO⁺ CSM calculations for direct J/ψ are demarcated by green dashed lines. The NLO⁺ CSM calculations are also extrapolated to the prompt production (hatched blue band). The NLO⁺ CSM does not predict significant p_T dependence, whereas the data exhibit it. The LO COM suggests rather a trend opposite to the data trend with the decreasing parameter λ_ϑ as p_T increases. However, both the STAR and the PHENIX results are consistent with mentioned models within experimental and theoretical uncertainties.

5.2 J/ψ and $\psi(2S)$ polarization measurements in $p\bar{p}$ collisions at $\sqrt{s} = 1.96 \text{ TeV}$ by the CDF experiments

The J/ψ and $\psi(2S)$ polarization measurements were performed at the CDF experiment in $p\bar{p}$ collisions at center-of-mass energy $\sqrt{s} = 1.96 \text{ TeV}$ [7]. Both vector mesons were detected in the dimuon decay channel. The mid-rapidity range $|y| < 0.6$ and p_T region from 5 to 30 GeVc^{-1} were explored.

The contribution of B meson decays was separated. The polarization parameter λ_ϑ (denoted in this measurement as α) was obtained for prompt J/ψ and $\psi(2S)$ in the HX frame. Measured p_T range was divided into six bins in the case of J/ψ , into three bins to the case of $\psi(2S)$. The experimentally obtained $\cos\vartheta$ distributions, integrated over the φ angle, were fitted with function in the equation (5.1), in each p_T bin.

Left and right panels of Figure 5.5 show the polarization parameter as a function of p_T for J/ψ and $\psi(2S)$, respectively. NRQCD from [26] and k_T -factorization from [15] predictions are marked by the blue bands and red lines, respectively. Both these models are for direct production. k_T -factorization predicts strong longitudinal polarization and covers only $p_T < 20 \text{ GeVc}^{-1}$ region in both cases, J/ψ and $\psi(2S)$. The NRQCD predicts λ_ϑ close to zero at 5 GeVc^{-1} in the J/ψ case. According to the NRQCD, λ_ϑ has increasing trend with rising p_T . The prediction at the same p_T value for $\psi(2S)$ is higher than for J/ψ .

The measured value of the J/ψ polarization parameter λ_ϑ is consistent with zero at the two first p_T bins. The parameter decreases with increasing p_T towards negative values. The measured $\psi(2S)$ polarization parameter λ_ϑ has a positive value at lowest p_T bin and with increasing p_T also decreases.

The NRQCD calculations reproduce J/ψ and $\psi(2S)$ cross sections at the Tevatron [7]. However, the NRQCD prediction for the polarization strongly differs from the trend of the measured data for both mesons. In the case of both mesons, the k_T -factorization predictions has the trend with decreasing value of λ_ϑ with rising p_T such as the data, nevertheless predicted values significantly underpredicts the measured values.

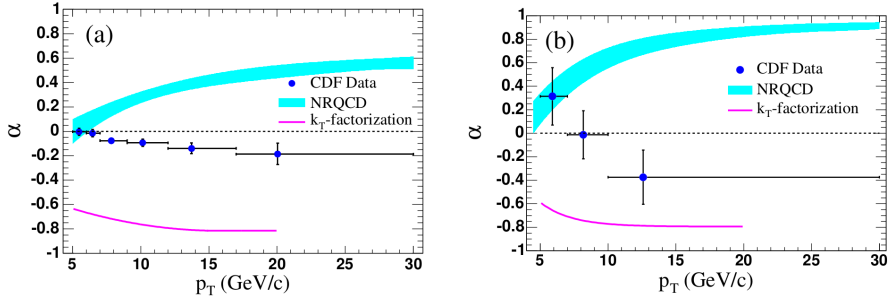


Figure 5.5: Results of the CDF experiment on the J/ψ and $\psi(2S)$ polarization in the HX frame compared to two model predictions. The polarization parameter λ_θ marked as α is shown as the function of p_T . The results for J/ψ are situated on the left, for $\psi(2S)$ on the right. NRQCD prediction is shown as blue area, k_T -factorization as red line. The figure is taken from [7].

5.3 J/ψ polarization measurements in pp collisions at $\sqrt{s} = 7$ TeV by the ALICE experiment

The inclusive J/ψ polarization was studied by the ALICE experiment in pp collisions with the center-of-mass energy of $\sqrt{s} = 7$ TeV [5]. The research was performed at the rapidity range of $2.5 < y < 4$ and for transverse momentum region $2 < p_T < 8$ GeV c^{-1} . J/ψ were detected in the dimuon decay channel.

The J/ψ polarization parameters λ_θ and λ_φ were studied in the HX and the CS frames. The parameters were obtained in three p_T bins, $2 < p_T < 3$ GeV c^{-1} , $3 < p_T < 4$ GeV c^{-1} and $4 < p_T < 8$ GeV c^{-1} . 2-D binning of $\cos \vartheta$ vs. φ distributions was not performed due to insufficient statistics for this purpose. Thus λ_θ and λ_φ were studied based on 1-D $\cos \vartheta$ and φ distributions integrated over φ and ϑ (4.5), respectively [5]. A simultaneous fit of $|\cos \vartheta|$ and $|\varphi|$ distributions was performed at $0 < |\cos \vartheta| < 0.8$ and $0 < |\varphi| < \pi/2$.

The measured values of the parameters can be seen in the Figure 5.6. The upper panel shows λ_θ in the CS and the HX frame. The parameter λ_φ in both frames is shown on the lower panel. The results on λ_θ and λ_φ are consistent with zero within uncertainties in both frames. The biggest deflection from zero value can be seen in the case of λ_θ at the lowest p_T bin. With increasing p_T measured value of λ_θ in the HX frame tends to zero. With the exception of mentioned case, measured data show no polarization. No azimuthal anisotropy was observed in both frames. λ_φ is close to zero for all p_T bins.

The difference between inclusive and prompt production in the polarization is estimated to be low (at most 0.05), however difference between prompt and direct production can be significant [5]. The NLO calculations ([42], [33]) for direct J/ψ polarization parameter λ_θ in HX frame via the colour-singlet

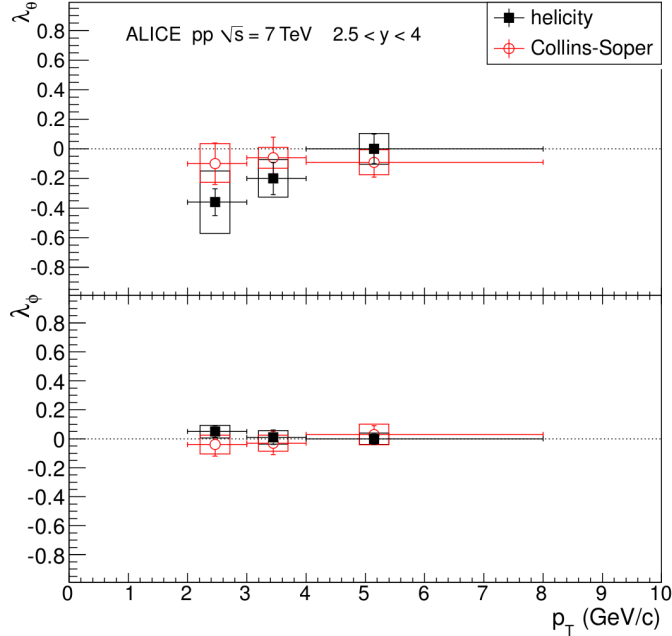


Figure 5.6: The results on the J/ψ polarization parameters vs. p_T performed by the ALICE experiment. λ_θ is shown in the top of figure, λ_ϕ in the bottom. The measurements were performed in the CS (red empty circles) and HX (black full squares) frames. The figure is taken from [5].

model exhibit strong longitudinal polarization at $p_T \sim 5 \text{ GeVc}^{-1}$ [5], which is in the contrast with discussed measurement. The S-wave colour-octet channels calculations from [33] show significant transverse polarization [5]. The prediction of [33] are not supported by the results on λ_θ presented by the ALICE collaboration. However, other calculations are needed to be done before more specific conclusions connected with the colour-octet model, for example to calculate the P-wave-channel contribution. More theoretical predictions are available now, since the ALICE paper was published.

5.4 J/ψ polarization measurements in pp collisions at $\sqrt{s} = 7 \text{ TeV}$ by the LHCb experiment

The prompt J/ψ polarization measurement was performed in the LHCb experiment in pp -collisions at $\sqrt{s} = 7 \text{ TeV}$ [2]. The J/ψ were detected via dimuon decay channel $J/\psi \rightarrow \mu^+ \mu^-$. The polarization parameters λ_θ , λ_ϕ and $\lambda_{\theta\phi}$

in the HX and the CS frame were studied at the rapidity range $2.0 < y < 4.5$ and p_T region $2 < p_T < 15$ GeV c^{-1} . The edges of p_T and y bins were [2, 3, 4, 5, 7, 10, 15] GeV c^{-1} and [2.0, 2.5, 3.0, 3.5, 4.0, 4.5] respectively.

The total angular distribution is (apart from normalization factor)

$$\frac{d^2 N}{d \cos \vartheta d \varphi} \propto 1 + \lambda_{\vartheta} \cos^2 \vartheta + \lambda_{\vartheta\varphi} \sin 2\vartheta \cos \varphi + \lambda_{\varphi} \sin^2 \vartheta \cos 2\varphi. \quad (5.2)$$

The data sample was big enough to perform 2-D binning and gain all three parameters λ_{ϑ} , λ_{φ} and $\lambda_{\vartheta\varphi}$ from (5.2). In the HX frame, the λ_{φ} and $\lambda_{\vartheta\varphi}$ were consistent with zero [2]. Thus we can consider HX frame to be the "natural" frame. λ_{ϑ} in the HX and the CS frame as the function of p_T for different y bins is shown in the Figure 5.7 on the left and on the right, respectively. λ_{ϑ} shows slight longitudinal polarization for the lowest p_T bins and rises mildly with rising p_T .

The deviation of λ_{ϑ} and λ_{φ} in the CS frame from zero was slightly larger than in HX frame but not significant. The λ_{φ} was positive in the most of bins (p_T vs. y). λ_{φ} was rather negative.

The results on λ_{ϑ} vs. p_T in the HX frame for $2.5 < y < 4.0$ are shown in the Figure 5.8 together with model predictions of the NLO CS ([19]) and NLO NRQCD ([19], [34], [21]) predictions. The NLO CS calculations are for direct J/ψ , whereas the NLO NRQCD include contribution from the $\psi(2S)$ and χ_c feed-down. The NLO CS predicts λ_{ϑ} decreasing with rising p_T and strong longitudinal polarization for $5 < p_T < 15$ GeV c^{-1} , which is in the disagreement with the LHCb measurement. There are three different NLO NRQCD calculations shown in the Figure 5.8. The best agreement with the data was found between the NRQCD prediction from [19] marked by green hatched area in the Figure 5.8.

$\psi(2S)$ polarization measurements were also presented by the LHCb in pp collisions at center-of-mass energy 7 TeV in the paper [4]. Measurements were performed for the $3.5 < p_T < 15$ GeV c^{-1} and $2.0 < y < 4.5$. Results on parameters λ_{ϑ} , λ_{φ} , $\lambda_{\vartheta\varphi}$ in the HX and the CS frame and $\tilde{\lambda}$ were obtained. There was observed slight negative polarization in the results on $\tilde{\lambda}$. No strong polarization was observed.

5.5 J/ψ and $\psi(2S)$ polarization measurements in pp collisions at $\sqrt{s} = 7$ TeV by the CMS experiment

The CMS experiment reported the prompt J/ψ and $\psi(2S)$ polarization measurement in pp collisions at 7 TeV [22]. J/ψ and $\psi(2S)$ were detected via dimuon decay channel. The measurements of J/ψ and $\psi(2S)$ were performed in the transverse momentum ranges of $14 < p_T < 70$ GeV and $14 < p_T < 50$ GeV, respectively. The data for J/ψ and $\psi(2S)$ polarization measurement were collected at $0.6 < |y| < 1.2$ and $1.2 < |y| < 1.5$ GeV, respectively.

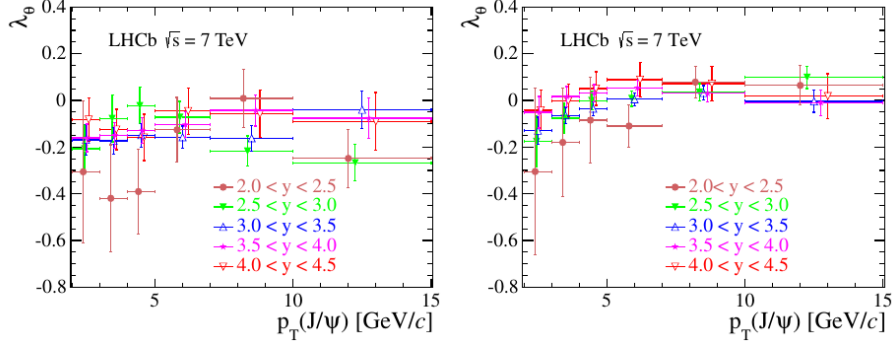


Figure 5.7: The results on the J/ψ polarization parameter λ_θ vs. p_T for different rapidity bins performed by the LHCb experiment. The left panel and the right panel of the figure shows λ_θ in the HX frame and in CS frame, respectively.

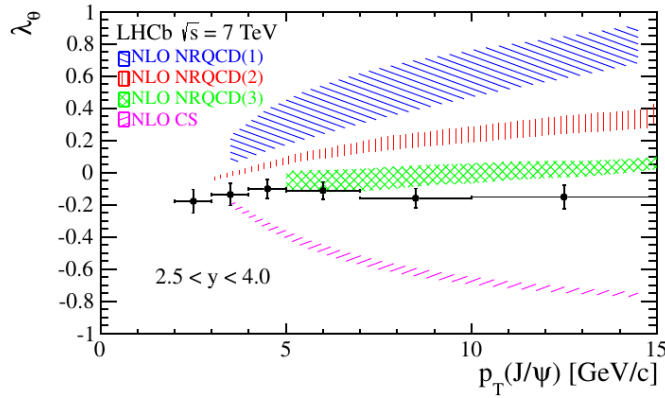


Figure 5.8: The results on the J/ψ polarization parameter λ_θ vs. p_T for the rapidity $2.5 < y < 4.0$ in the HX frame. The measurement performed at the LHCb experiment is compared to the NLO CS model from [19] (pink diagonal lines) and the NLO NRQCD predictions from [19] (blue diagonal lines), [34] (red vertical lines) and [21] (green hatched).

Polarization parameters λ_φ , λ_ϑ and $\lambda_{\vartheta\varphi}$ from the dilepton decay angular distribution (4.2) were studied in three frames, the HX, the CS and the PX (the perpendicular helicity frame) [22]. The parameters were obtained by fitting 2-D distributions, $\cos\vartheta$ vs. φ . They calculated also the frame invariant parameter $\tilde{\lambda}$ defined by the equation (4.15).

The results on parameters λ_ϑ , λ_φ and $\lambda_{\vartheta\varphi}$ in the HX frame as a function of p_T for several $|y|$ bins, for both vector mesons are shown in the Figure 5.9. The J/ψ and $\psi(2S)$ results for different rapidity ranges are on the left and on the right hand-side, respectively. The measured parameters λ_φ and $\lambda_{\vartheta\varphi}$ in the HX frame for different rapidity ranges are very close to zero. The λ_ϑ is more deflected from zero, but not significantly, and has slight positive values. The results on λ_ϑ in the HX frame are compared to the NLO NRQCD calculations for $|y| < 2.4$ from [40]. The calculations are performed for prompt J/ψ and $\psi(2S)$ and are shown in the Figure 5.9 as green lines. Green dashed lines mark an estimate for the theoretical uncertainty. The measured λ_ϑ is in disagreement with the mentioned NLO NRQCD predictions.

The experimentally extracted frame-independent parameter $\tilde{\lambda}$ as a function of p_T in the rapidity range $|y| < 0.6$, in the HX, the CS and the PX frame for J/ψ and $\psi(2S)$ is shown in the Figure 5.10. The results on $\tilde{\lambda}$ in all three frames are in good agreement. The good agreement is also seen in the cases of the other measured $|y|$ bins [22]. In the other words, no unaccounted systematic effects are observed.

The measured parameter $\tilde{\lambda}$ shows no strong polarization in all $|y|$ ranges. The other parameters, λ_ϑ , λ_φ and $\lambda_{\vartheta\varphi}$, are also close to zero in all frames used for measurement. Thus, strong polarization in the kinematic region studied by the CMS can be excluded [22].

5.6 $\Upsilon(1S)$, $\Upsilon(2S)$ and $\Upsilon(3S)$ polarization measurements in pp collisions at $\sqrt{s} = 7$ TeV by the CMS experiment

The polarization of inclusive $\Upsilon(1S)$, $\Upsilon(2S)$ and $\Upsilon(3S)$ was studied at the CMS experiment [23]. $\Upsilon(nS)$ were detected via dimuon decay channel in pp collisions at $\sqrt{s} = 7$ GeV. $\Upsilon(1S)$, $\Upsilon(2S)$ and $\Upsilon(3S)$ with $10 < p_T < 50$ GeV and $|y| < 1.2$ were measured. The analysed data sample was divided to two rapidity ranges $|y| < 0.6$ and $0.6 < |y| < 1.2$, for which results were presented.

The polarization parameters λ_ϑ , λ_φ , $\lambda_{\vartheta\varphi}$ and the frame-independent parameter $\tilde{\lambda}$ were studied in three frames, the HX, the PX and the CS. The analysis was performed using unbinned likelihood approach [23].

The parameters λ_ϑ , λ_φ and $\lambda_{\vartheta\varphi}$ vs. p_T in the HX frame for measured $\Upsilon(nS)$ states in the rapidity range $|y| < 0.6$ can be seen in the Figure 5.11. These results are consistent with zero, especially λ_φ and $\lambda_{\vartheta\varphi}$ are very close to zero and have relatively small uncertainties. The λ_ϑ shows slight transverse polarization for all three measured $\Upsilon(nS)$ states. Similar values were obtained in the rapidity region

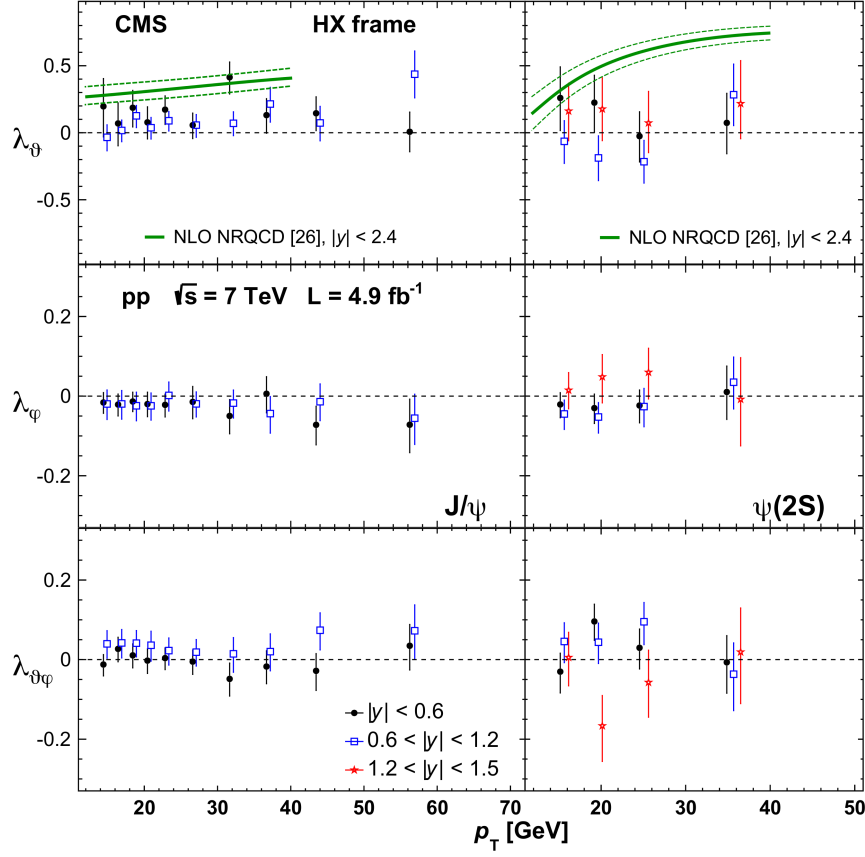


Figure 5.9: The polarization parameters λ_θ , λ_ϕ and $\lambda_{\phi\theta}$ (from top to bottom) as a function of p_T measured by the CMS experiment in the HX frame. The results on J/ψ in the rapidity ranges $|y| < 0.6$, $0.6 < |y| < 1.2$ and $\psi(2S)$ in the rapidity ranges $|y| < 0.6$, $0.6 < |y| < 1.2$ $1.2 < |y| < 1.5$ are depicted on the left and on the right, respectively. The error bars correspond to total uncertainty (at 68.3% CL). The measured parameter λ_θ is compared to the NLO NRQCD results for prompt vector mesons from [40] marked by green line. The model uncertainties are marked by green dashed lines. The Figure is taken from [22].

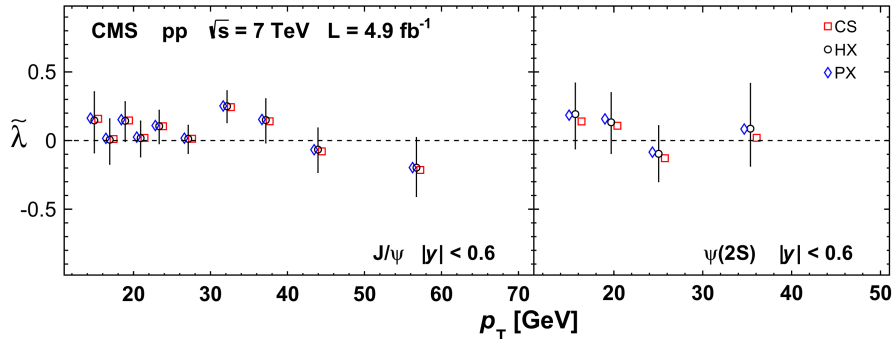


Figure 5.10: The frame-independent parameter $\tilde{\lambda}$ as a function of p_T measured by the CMS experiment in the CS, the HX and the PX frame. The left and right panel shows $\tilde{\lambda}$ for J/ψ and $\psi(2S)$, respectively. The J/ψ and $\psi(2S)$ sample with $|y| < 0.6$ was used for calculation of $\tilde{\lambda}$. The Figure is taken from [22].

of $0.6 < |y| < 1.2$ [23].

The results on the frame-independent parameter $\tilde{\lambda}$ vs. p_T in all explored frames and both rapidity ranges for all measured $\Upsilon(nS)$ states are depicted in the Figure 5.12. As can be seen, the results on $\tilde{\lambda}$ are in good agreement in all studied frames. The $\tilde{\lambda}$ is compatible with zero. A slight transverse polarization can be seen in the case of rapidity range $|y| < 0.6$ and $\Upsilon(2S)$ and $\Upsilon(3S)$.

All the polarization parameters are consistent with zero or are slightly deflected from the zero, thus strong polarization in any frame is excluded [23]. This result supports that the $\Upsilon(nS)$ states are probably created as unpolarized mixture in pp collisions at 7 GeV. However, feed-down from other bottomium states is not extracted. Therefore, clear conclusion for the direct production of $\Upsilon(nS)$ states can not be done.

$\Upsilon(nS)$ states are better test of non-relativistic calculations than charmonia, because bottomia are significantly heavier. The NRQCD calculation [16] predicts strong transverse polarization, which strongly disagrees with the CMS results on $\Upsilon(nS)$ polarization [23].

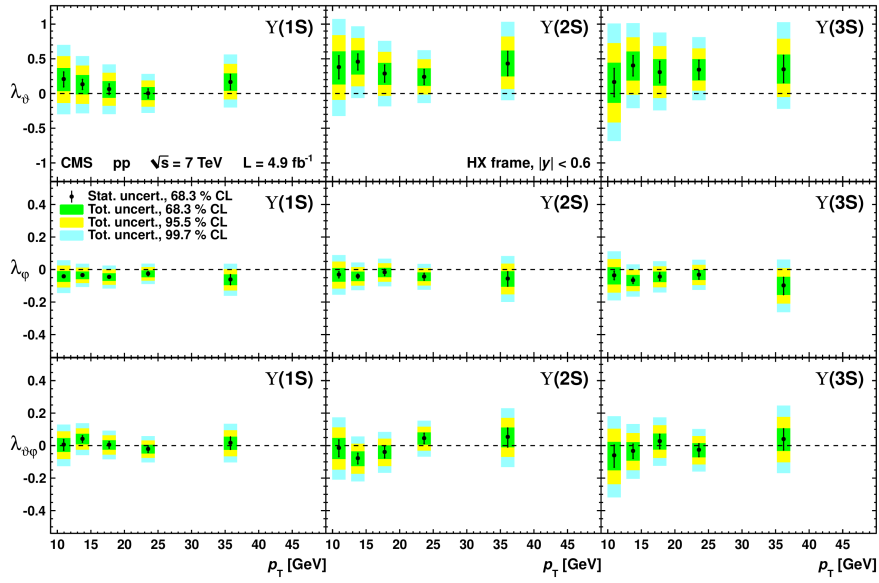


Figure 5.11: The polarization parameters for $\Upsilon(1S)$, $\Upsilon(2S)$ and $\Upsilon(3S)$ (from left to right) λ_{θ} , λ_{ϕ} and $\lambda_{\theta\phi}$ (from top to bottom) as a function of p_T measured by the CMS experiment in the HX frame. The results on $\Upsilon(nS)$ in the rapidity range $|y| < 0.6$. The error bars correspond to total uncertainty (68.3%, 95.5%, 99.7% CL). The model uncertainties are marked by green dashed lines. The Figure is taken from [23].

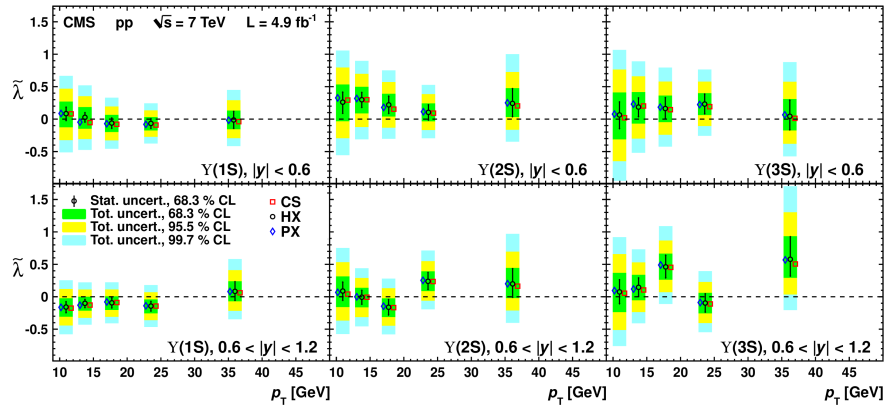


Figure 5.12: The frame-independent parameter $\tilde{\lambda}$ for $\Upsilon(1S)$, $\Upsilon(2S)$ and $\Upsilon(3S)$ (from left to right) as a function of p_T measured by the CMS experiment in the CS, the HX and the PX frame. The top and bottom panel shows $\tilde{\lambda}$ for rapidity range $|y| < 0.6$ and $|y| < 1.2$, respectively. The error bars indicate to total uncertainty (68.3%, 95.5%, 99.7% CL) The Figure is taken from [23].

Conclusion

Quarkonia are important for studying QCD mechanisms. They are also abundantly used for analyses of collisions. However, exact quarkonium production mechanism is not known. There are theoretical models predicting observables that can be measured in an experiment. Besides cross section, the polarization of quarkonia provides opportunity to distinguish between theoretical models

Basic theoretical approaches to quarkonium production quarkonium and approaches to polarization measurements were discussed. The performed measurements of quarkonium polarization in pp and $p\bar{p}$ collisions were presented in the thesis and were compared to some model predictions.

The total angular dilepton distribution is determined by three polarization parameters, λ_ϑ , λ_φ and $\lambda_{\vartheta\varphi}$. The polarization parameters are usually measured in the HX, the GJ, the CS or the PX frame and are presented as the functions of p_T . Useful is also frame invariant parameter $\tilde{\lambda}$, which helps us with comparing results obtained in different reference frames and draw frame-independent conclusions.

J/ψ polarization measurements by the STAR, the PHENIX, the CDF, the ALICE, the LHCb and the CMS were presented in the thesis. Most of measurements showed slight polarization. This fact is in a disagreement with models predicting strong polarization. However, we have to take into the account also that some model predictions are performed only for direct production, whereas they are compared to measurements with contribution from the feed-down of charmonium states with higher mass or B mesons. The results presented firstly in the thesis were only for λ_ϑ parameter. Other parameters, λ_φ and $\lambda_{\vartheta\varphi}$ was obtained from the measurements with broader data sample performed at the LHCb and the CMS. $\psi(2S)$ polarization measurements were presented by the CDF, the CMS and the LHCb. No strong polarization was observed, but for example in the LHCb case, slight negative polarization was seen. The results on $\Upsilon(1S)$, $\Upsilon(2S)$ and $\Upsilon(3S)$ by the CMS were discussed in the thesis.

Presented measurements are important for quarkonium-polarization studies. However, more measurement have to be done before making more specific conclusions. For example bigger data sample would be suitable for obtaining more precise results. There are another p_T and y regions to be explored. Studying of both, charmonium and bottomium states, is useful, because it is supposed that there are different contributions from a feed-down for different quarkonium states. Overall, here are many opportunities for next measurements

of the quarkonium polarization.

Bibliography

- [1] Georges Aad et al. “Observation of a new particle in the search for the Standard Model Higgs boson with the ATLAS detector at the LHC”. In: *Phys.Lett.* B716 (2012), pp. 1–29. DOI: 10.1016/j.physletb.2012.08.020. arXiv: 1207.7214 [hep-ex].
- [2] R Aaij et al. “Measurement of J/ψ polarization in pp collisions at $\sqrt{s} = 7$ TeV”. In: *Eur.Phys.J.* C73.11 (2013), p. 2631. DOI: 10.1140/epjc/s10052-013-2631-3. arXiv: 1307.6379 [hep-ex].
- [3] R. Aaij et al. “Measurement of J/ψ production in pp collisions at $\sqrt{s} = 7$ TeV”. In: *Eur.Phys.J.* C71 (2011), p. 1645. DOI: 10.1140/epjc/s10052-011-1645-y. arXiv: 1103.0423 [hep-ex].
- [4] Roel Aaij et al. “Measurement of $\psi(2S)$ polarisation in pp collisions at $\sqrt{s} = 7$ TeV”. In: *Eur.Phys.J.* C74.5 (2014), p. 2872. DOI: 10.1140/epjc/s10052-014-2872-9. arXiv: 1403.1339 [hep-ex].
- [5] Betty Abelev et al. “ J/ψ polarization in pp collisions at $\sqrt{s} = 7$ TeV”. In: *Phys.Rev.Lett.* 108 (2012), p. 082001. DOI: 10.1103/PhysRevLett.108.082001. arXiv: 1111.1630 [hep-ex].
- [6] G. S. Abrams et al. “Discovery of a Second Narrow Resonance in $e+e$ -Annihilation”. In: *Phys.Rev.Lett.* (1974). DOI: 10.1103/PhysRevLett.33.1453.
- [7] A. Abulencia et al. “Polarization of J/ψ and ψ_{2S} mesons produced in $p\bar{p}$ collisions at $\sqrt{s} = 1.96$ -TeV”. In: *Phys.Rev.Lett.* 99 (2007), p. 132001. DOI: 10.1103/PhysRevLett.99.132001. arXiv: 0704.0638 [hep-ex].
- [8] L. Adamczyk et al. “ J/ψ polarization in p+p collisions at $\sqrt{s} = 200$ GeV in STAR”. In: *Phys.Lett.* B739 (2014), pp. 180–188. DOI: 10.1016/j.physletb.2014.10.049. arXiv: 1311.1621 [nucl-ex].
- [9] A. Adare et al. “Transverse momentum dependence of J/ψ polarization at midrapidity in p+p collisions at $s^{*}(1/2) = 200$ -GeV”. In: *Phys.Rev.* D82 (2010), p. 012001. DOI: 10.1103/PhysRevD.82.012001. arXiv: 0912.2082 [hep-ex].
- [10] A. Andronic et al. “Heavy-flavour and quarkonium production in the LHC era: from proton-proton to heavy-ion collisions”. In: (2015). arXiv: 1506.03981 [nucl-ex].

- [11] P. Artoisenet, J.P. Lansberg, and F. Maltoni. “Hadroproduction of J/ψ and v in association with a heavy-quark pair”. In: *Phys.Lett.* B653 (2007), pp. 60–66. DOI: 10.1016/j.physletb.2007.04.031. arXiv: hep-ph/0703129 [HEP-PH].
- [12] P. Artoisenet et al. “ Υ Production at Fermilab Tevatron and LHC Energies”. In: *Phys.Rev.Lett.* 101 (2008), p. 152001. DOI: 10.1103/PhysRevLett.101.152001. arXiv: 0806.3282 [hep-ph].
- [13] J.J. Aubert et al. “Experimental Observation of a Heavy Particle J”. In: *Phys.Rev.Lett.* 33 (1974), pp. 1404–1406. DOI: 10.1103/PhysRevLett.33.1404.
- [14] J.E. Augustin et al. “Discovery of a Narrow Resonance in $e^+ e^-$ Annihilation”. In: *Phys.Rev.Lett.* 33 (1974), pp. 1406–1408. DOI: 10.1103/PhysRevLett.33.1406.
- [15] S. P. Baranov. “Highlights from the k_T factorization approach on the quarkonium production puzzles”. In: *Phys.Rev.* D66 (2002), p. 114003. DOI: 10.1103/PhysRevD.66.114003.
- [16] Geoffrey T. Bodwin, Eric Braaten, and G. Peter Lepage. “Rigorous QCD analysis of inclusive annihilation and production of heavy quarkonium”. In: *Phys.Rev.* D51 (1995), pp. 1125–1171. DOI: 10.1103/PhysRevD.51.5853, 10.1103/PhysRevD.51.1125. arXiv: hep-ph/9407339 [hep-ph].
- [17] Daniel Boer and Cristian Pisano. “Polarized gluon studies with charmonium and bottomonium at LHCb and AFTER”. In: *Phys.Rev.* D86 (2012), p. 094007. DOI: 10.1103/PhysRevD.86.094007. arXiv: 1208.3642 [hep-ph].
- [18] N. Brambilla et al. “Heavy quarkonium: progress, puzzles, and opportunities”. In: *Eur.Phys.J.* C71 (2011), p. 1534. DOI: 10.1140/epjc/s10052-010-1534-9. arXiv: 1010.5827 [hep-ph].
- [19] Mathias Butenschoen and Bernd A. Kniehl. “ J/ψ polarization at Tevatron and LHC: Nonrelativistic-QCD factorization at the crossroads”. In: *Phys.Rev.Lett.* 108 (2012), p. 172002. DOI: 10.1103/PhysRevLett.108.172002. arXiv: 1201.1872 [hep-ph].
- [20] John M. Campbell, F. Maltoni, and F. Tramontano. “QCD corrections to J/ψ and Upsilon production at hadron colliders”. In: *Phys.Rev.Lett.* 98 (2007), p. 252002. DOI: 10.1103/PhysRevLett.98.252002. arXiv: hep-ph/0703113 [HEP-PH].
- [21] Kuang-Ta Chao et al. “ J/ψ Polarization at Hadron Colliders in Nonrelativistic QCD”. In: *Phys.Rev.Lett.* 108 (2012), p. 242004. DOI: 10.1103/PhysRevLett.108.242004. arXiv: 1201.2675 [hep-ph].
- [22] Serguei Chatrchyan et al. “Measurement of the prompt J/ψ and $\psi(2S)$ polarizations in pp collisions at $\sqrt{s} = 7$ TeV”. In: *Phys.Lett.* B727 (2013), pp. 381–402. DOI: 10.1016/j.physletb.2013.10.055. arXiv: 1307.6070 [hep-ex].

- [23] Serguei Chatrchyan et al. “Measurement of the $Y(1S)$, $Y(2S)$ and $Y(3S)$ polarizations in pp collisions at $\sqrt{s} = 7$ TeV”. In: *Phys.Rev.Lett.* 110.8 (2013), p. 081802. DOI: 10.1103/PhysRevLett.110.081802. arXiv: 1209.2922 [hep-ex].
- [24] Serguei Chatrchyan et al. “Observation of a new boson at a mass of 125 GeV with the CMS experiment at the LHC”. In: *Phys.Lett.* B716 (2012), pp. 30–61. DOI: 10.1016/j.physletb.2012.08.021. arXiv: 1207.7235 [hep-ex].
- [25] Serguei Chatrchyan et al. “Observation of sequential Upsilon suppression in PbPb collisions”. In: *Phys.Rev.Lett.* 109 (2012), p. 222301. DOI: 10.1103/PhysRevLett.109.222301. arXiv: 1208.2826 [nucl-ex].
- [26] Peter L. Cho and Mark B. Wise. “Spin symmetry predictions for heavy quarkonia alignment”. In: *Phys.Lett.* B346 (1995), pp. 129–136. DOI: 10.1016/0370-2693(94)01658-Y. arXiv: hep-ph/9411303 [hep-ph].
- [27] Hee Sok Chung et al. “Polarization of prompt J/ψ in proton-proton collisions at RHIC”. In: *Phys.Rev.* D81 (2010), p. 014020. DOI: 10.1103/PhysRevD.81.014020. arXiv: 0911.2113 [hep-ph].
- [28] G. C. Contreras. *Interaction of Particles with Matter*. Presentation, 2014.
- [29] P. Faccioli. “Angular momentum and decay distribution in high energy physics: an introduction and use cases for the LHC”. In: *Presentation at CERN* (2013).
- [30] P. Faccioli, C. Lourenco, and J. Seixas. “A New approach to quarkonium polarization studies”. In: *Phys.Rev.* D81 (2010), p. 111502. DOI: 10.1103/PhysRevD.81.111502. arXiv: 1005.2855 [hep-ph].
- [31] P. Faccioli et al. “Towards the experimental clarification of quarkonium polarization”. In: *Eur.Phys.J.* C69 (2010), pp. 657–673. DOI: 10.1140/epjc/s10052-010-1420-5. arXiv: 1006.2738 [hep-ph].
- [32] Anthony D. Frawley, T. Ullrich, and R. Vogt. “Heavy flavor in heavy-ion collisions at RHIC and RHIC II”. In: *Phys.Rept.* 462 (2008), pp. 125–175. DOI: 10.1016/j.physrep.2008.04.002. arXiv: 0806.1013 [nucl-ex].
- [33] Bin Gong and Jian-Xiong Wang. “QCD corrections to polarization of J/ψ and ψ at Tevatron and LHC”. In: *Phys.Rev.* D78 (2008), p. 074011. DOI: 10.1103/PhysRevD.78.074011. arXiv: 0805.2469 [hep-ph].
- [34] Bin Gong et al. “Polarization for Prompt J/ψ and $\psi(2S)$ Production at the Tevatron and LHC”. In: *Phys.Rev.Lett.* 110.4 (2013), p. 042002. DOI: 10.1103/PhysRevLett.110.042002. arXiv: 1205.6682 [hep-ph].
- [35] P. Hagler et al. “Towards a solution of the charmonium production controversy: k^- perpendicular factorization versus color octet mechanism”. In: *Phys.Rev.Lett.* 86 (2001), pp. 1446–1449. DOI: 10.1103/PhysRevLett.86.1446. arXiv: hep-ph/0004263 [hep-ph].

- [36] S. W. Herb et al. “Observation of a Dimuon Resonance at 9.5 GeV in 400GeV Proton-Nucleus Collisions”. In: *Phys.Rev.Lett.* (1977). DOI: 10.1103/PhysRevLett.39.252.
- [37] W. R. Innes et al. “Structure in the Upsilon Region”. In: *Phys.Rev.Lett.* (1977). DOI: 10.1103/PhysRevLett.39.1240.
- [38] Zhong-Bo Kang, Yan-Qing Ma, and Raju Venugopalan. “Quarkonium production in high energy proton-nucleus collisions: CGC meets NRQCD”. In: *JHEP* 1401 (2014), p. 056. DOI: 10.1007/JHEP01(2014)056. arXiv: 1309.7337 [hep-ph].
- [39] Vardan Khachatryan et al. “Constraints on parton distribution functions and extraction of the strong coupling constant from the inclusive jet cross section in pp collisions at $\sqrt{s} = 7$ TeV”. In: (2014). arXiv: 1410.6765 [hep-ex].
- [40] Vardan Khachatryan et al. “Prompt and non-prompt J/ψ production in pp collisions at $\sqrt{s} = 7$ TeV”. In: *Eur.Phys.J.* C71 (2011), p. 1575. DOI: 10.1140/epjc/s10052-011-1575-8. arXiv: 1011.4193 [hep-ex].
- [41] J.P. Lansberg. “ J/ψ , ψ' and ψ production at hadron colliders: A Review”. In: *Int.J.Mod.Phys.* A21 (2006), pp. 3857–3916. DOI: 10.1142/S0217751X06033180. arXiv: hep-ph/0602091 [hep-ph].
- [42] J.P. Lansberg. “On the mechanisms of heavy-quarkonium hadroproduction”. In: *Eur.Phys.J.* C61 (2009), pp. 693–703. DOI: 10.1140/epjc/s10052-008-0826-9. arXiv: 0811.4005 [hep-ph].
- [43] J.P. Lansberg. “QCD corrections to polarisation in pp collisions at RHIC”. In: *Physics Letters B* 695.1â“4 (2011), pp. 149–156. ISSN: 0370-2693. DOI: <http://dx.doi.org/10.1016/j.physletb.2010.10.054>. URL: <http://www.sciencedirect.com/science/article/pii/S0370269310012657>.
- [44] Yun-peng Liu et al. “ J/ψ Transverse Momentum Distribution in High Energy Nuclear Collisions at RHIC”. In: *Phys.Lett.* B678 (2009), pp. 72–76. DOI: 10.1016/j.physletb.2009.06.006. arXiv: 0901.2757 [nucl-th].
- [45] Yan-Qing Ma, Kai Wang, and Kuang-Ta Chao. “ $J/\psi(\psi')$ production at the Tevatron and LHC at $\mathcal{O}(\alpha_s^4 v^4)$ in nonrelativistic QCD”. In: *Phys.Rev.Lett.* 106 (2011), p. 042002. DOI: 10.1103/PhysRevLett.106.042002. arXiv: 1009.3655 [hep-ph].
- [46] B. R. Martin. *Nuclear and particle physics: An Introduction*. John Wiley and Sons, 2006.
- [47] T. Matsui and H. Satz. “ J/ψ Suppression by Quark-Gluon Plasma Formation”. In: *Phys.Lett.* B178 (1986), p. 416. DOI: 10.1016/0370-2693(86)91404-8.
- [48] Agnes Mocsy. “Potential Models for Quarkonia”. In: *Eur.Phys.J.* C61 (2009), pp. 705–710. DOI: 10.1140/epjc/s10052-008-0847-4. arXiv: 0811.0337 [hep-ph].

- [49] K. A. Olive and others (Particle Data Group). “Gauge and Higgs Bosons (γ , g , W , Z , \dots)” In: *Chin. Phys. C* 38, 090001 (2014).
- [50] K. A. Olive and others (Particle Data Group). “Mesons”. In: *Chin. Phys. C* 38, 090001 (2014).
- [51] S. Eidelman et al. (Particle Data Group Collaboration). In: *Phys. Lett. B* 592 (2004).
- [52] V. Petracek. *Subatomova fyzika I*. 2009. URL: <http://physics.fjfi.cvut.cz/files/predmety/02SF/common/subatomovka-book-obr-zc12.2.10.pdf>.
- [53] G. Roland, K. Safarik, and P. Steinberg. “Heavy-ion collisions at the LHC”. In: *Prog.Part.Nucl.Phys.* 77 (2014), pp. 70–127. DOI: 10.1016/j.pnpnp.2014.05.001.
- [54] G. P. Shaw and B. R. Martin. *Particle Physics*. John Wiley and Sons, 2008.
- [55] “Standard Model”. In: *Wikipedia.org* (13.4.2015). URL: http://en.wikipedia.org/wiki/Standard_Model.
- [56] S. Ting. “The Discovery of the J Particle”. In: *Nobelprize.org* 1976 (1976), p. 28. URL: http://www.nobelprize.org/nobel_prizes/physics/laureates/1976/ting-lecture.pdf.
- [57] B. A. Trzeciak. “Polarization of hidden charm particles in relativistic proton-proton collisions measured in the STAR experiment”. In: *Phd. Thesis* (2013).
- [58] Barbara Trzeciak. “Heavy flavor production in the STAR experiment”. In: (2014). DOI: 10.1088/1742-6596/535/1/012021. arXiv: 1409.3410 [nucl-ex].
- [59] Barbara Trzeciak. “Quarkonia production in the STAR experiment”. In: *Nucl.Phys.* A904-905 (2013), pp. 607c–610c. DOI: 10.1016/j.nuclphysa.2013.02.087. arXiv: 1302.7293 [hep-ex].
- [60] T. Ullrich. “From Discovery to Exploration: Determining the Properties of Quark-Gluon Plasma”. In: *Presentation at Czech Technical University, Prague* (2009).
- [61] Xingbo Zhao and Ralf Rapp. “Charmonium in Medium: From Correlators to Experiment”. In: *Phys.Rev.* C82 (2010), p. 064905. DOI: 10.1103/PhysRevC.82.064905. arXiv: 1008.5328 [hep-ph].